Understanding hippocampal network dynamics by studying sharp-wave ripples across the proximal–distal axis of area CA1

A thesis submitted towards partial fulfilment of

BS-MS Dual Degree Programme

by

Mekhala Kumar (20131075)

Under the guidance of

Dr. Sachin Deshmukh

at the

Centre for Neuroscience,

Indian Institute of Science, Bangalore

Certificate

This is to certify that this dissertation entitled '**Understanding hippocampal network dynamics by studying sharp-wave ripples across the proximal–distal axis of area CA1**' towards the partial fulfilment of the BS-MS dual degree programme at the Indian Institute of Science Education and Research, Pune represents study/work carried out by **Mekhala Kumar** at **Indian Institute of Science, Bangalore** under the supervision of **Dr. Sachin Deshmukh, Centre for Neuroscience, Indian Institute of Science, Bangalore** during the academic year **2017-2018**.

Signature of Student

Signature of Supervisor

Date: 30/03/2018

Declaration

I hereby declare that the matter embodied in the report entitled '**Understanding hippocampal network dynamics by studying sharp-wave ripples across the proximal–distal axis of area CA1**' are the results of the work carried out by me at the **Centre for Neuroscience, Indian Institute of Science, Bangalore** under the supervision of **Dr. Sachin Deshmukh**, and the same has not been submitted elsewhere for any other degree.

Signature of Student

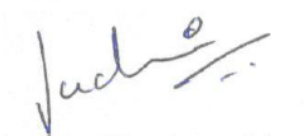

Signature of Supervisor

Date: 30/03/2018

CONTENTS

ABSTRACT

The area CA1 in the hippocampus is known to have qualitatively different inputs between the proximal and distal regions. Differences corresponding to these differing input patterns have been seen in the functional aspects of area CA1 across the proximal-distal axis. There might be differences in the networks that connect to the proximal and distal regions of area CA1 that encode and consolidate these memories. Sharp-wave ripples (SWR) in the area CA1 of the hippocampus reflect the activity of neurons at a network level. To study possible differences in the activity of the networks that connect to area CA1 across its proximal-distal axis, we recorded and analysed SWR across the proximal-distal axis of area CA1. We found that when SWR occur in one region of area CA1, there was a reduction in the likelihood of co-occurrence and in the relative amplitude of ripples as a function of distance from that region. Interestingly, we found that the difference in ripple peak time did not follow a similar trend; when SWR occurred in any region, the corresponding ripples in the distal region seemed to occur earlier while those in the proximal region seemed to occur later. Although our result regarding difference in peak time is ambiguous, our results on co-occurrence of SWR and relative ripple amplitudes across the proximal-distal axis imply that SWR initiated in one region of area CA1 progress to the other regions, and that the extent to which they progress depends on the distance from the region of initiation. These results are indicative of the possible differences in the connectivity and activity of the underlying networks that connect to area CA1.

LIST OF FIGURES

ACKNOWLEDGEMENTS

I would like to sincerely thank Dr. Sachin Deshmukh for his constant guidance throughout the course of the project. He has given me the opportunity and freedom to think of ways to approach various problems and has encouraged and patiently guided me through this process. His insights have been extremely valuable and essential to the successful completion of the project.

I would also like to thank Dr. Raghav Rajan for his useful insights on how I could improve some of my methods of analysis.

I am extremely thankful to Rajat Saxena for his valuable assistance over the course of the project. I am also very grateful to Harini Suri for having borne with my incessant questions regarding MATLAB, and for having been a daily source of entertainment. I am greatly indebted to my family for having tirelessly supported and encouraged me throughout the course of the project.

I would like to thank IISER, Pune for giving me the opportunity work in Dr. Sachin Deshmukh's lab at IISc, Bangalore

INTRODUCTION

The hippocampus is a structure in the medial temporal lobe of the brain that is known to play a role in the formation and recall of memories (Scoville and Milner, 1957). Studies using rodents as a model system have shown that the hippocampus has neurons that fire at specific locations, known as 'place cells' (O'Keefe, 1976). These neurons have been found to encode space in conjunction with non-spatial information (Moita et al., 2003; Komorowski et al., 2009), and also sequentially in time (Skaggs et al., 1996). Thus, the hippocampus is believed to encode episodic memory, which is the memory of events in terms of 'what happened', 'where', and 'when'.

The structure of the hippocampal formation in the rat is C-shaped, and is divided into three regions, namely, the dentate gyrus (DG), the hippocampus proper, and the subiculum. The hippocampus proper is further sub-divided into the *Cornu Ammonis* (CA) regions – CA1, CA2, and CA3. Areas CA1 and CA3 are each divided into proximal and distal regions, the proximal region being defined as the region closer to the DG and the distal region as that region that is further away from the DG. There is no clear boundary distinguishing the two regions; the region between the proximal and distal regions is called the intermediate region.

The hippocampus receives input from multiple sensory modalities via the lateral entorhinal cortex (LEC), and visuo-spatial input via the medial entorhinal cortex (MEC). The connections from the two entorhinal cortical regions converge in area CA3, but are concentrated towards the distal part of area CA3 (Ishizuka et al., 1990; Li et al., 1994). Area CA3 gives rise to projections to area CA1 via Schaffer collaterals, and also associational (recurrent) projections to area CA3 itself. This recurrent connectivity pattern is non-uniform along the proximal-distal axis of area CA3 – distal and intermediate CA3 have a greater density of recurrent connectivity than proximal CA3; projections from proximal CA3 to CA3 are relatively few and more localised to proximal CA3. The recurrent projections from distal and intermediate CA3 extend throughout the proximal-distal axis of area CA3 but are concentrated more towards the distal region of area CA3 (Ishizuka et al., 1990; Li et al., 1994; reviewed by Witter, 2007). Projections from area CA3 to area

CA1 and entorhinal cortex to area CA1 are segregated along the proximal-distal axis (Fig. 1) – the LEC and proximal part of CA3 project to distal CA1, and the MEC and distal part of CA3 project to proximal CA1. This pattern of segregation is maintained in the projections from area CA1 to the entorhinal cortex – proximal CA1 projects to the MEC while distal CA1 projects to the LEC (Naber et al., 2001; Tamamaki and Nojyo, 1995; reviewed by van Strien et al., 2009). Thus, the inputs and outputs of proximal and distal CA1 are qualitatively different. Proximal CA1 and distal CA1 are believed to encode information differently (Henriksen et al., 2010; Igarashi et al., 2014; Nakazawa et al., 2016).

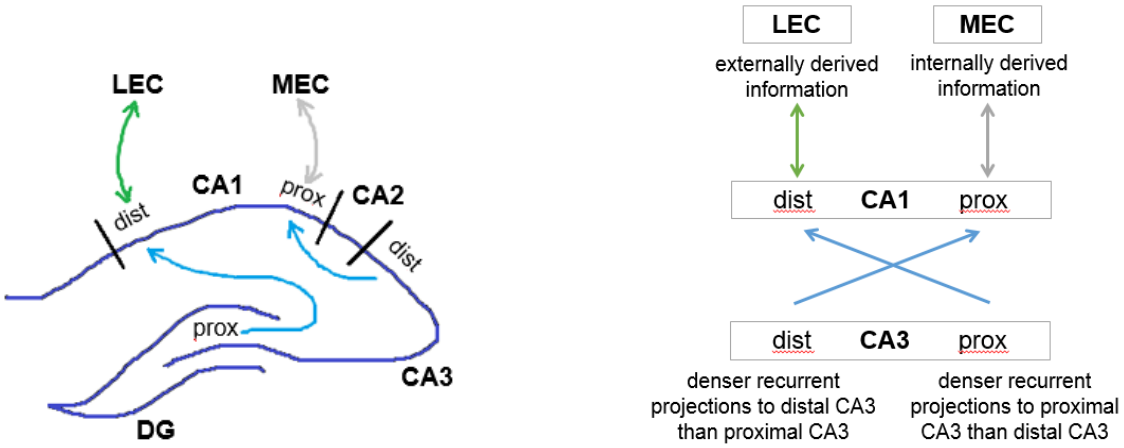

Fig. 1. Segregation in connectivity patterns along the proximal-distal axis of area CA1 from area CA3 and the entorhinal cortex

Functional differences in area CA1 corresponding to the connectivity pattern across the proximal-distal axis (also called the transverse axis) have been observed. For instance, in a study by Henriksen et al. (2010), it was shown that place cells in proximal CA1 have fewer and smaller place fields, while place cells in distal CA1 have more and larger place fields i.e. place cells in proximal CA1 are more spatially specific than those in distal CA1. On the other hand, in a task that involved associating odour and location, neurons in distal CA1 have been shown to develop greater selectivity for odours as compared to those in proximal CA1 (Igarashi et al., 2014). Memory retrieval in the context of fear conditioning has also been shown to differ across the proximal-distal axis. Nakazawa et al. (2016) have shown, using c-Fos expression in the mouse hippocampus, that the proportion of

neurons reactivated in a fear context with respect to the number of neurons active during the initial exposure to the fear context is greater in proximal CA1 than distal CA1. Additionally, they separately lesioned the proximal and distal CA1 and studied its effect on the reactivation of neurons during contextual fear conditioning. They found that a lesion to distal CA1 neither affected the reactivation of neurons in proximal CA1 nor the recall of the context fear memory, while a lesion to proximal CA1 showed an impairment in the recall of the context fear memory although neuronal activity was unaffected in distal CA1. This clearly indicates that the retrieval of contextual memories involves proximal CA1 but not distal CA1. These studies suggest that there may be some differences in the networks that connect to area CA1 along its proximal-distal axis.

We observed, during hippocampal neural recordings, that there were differences in occurrence of a certain kind of brain rhythm known as sharp-wave ripples (SWR) across the proximal-distal axis of area CA1 (unpublished data from Dr. James Knierim's lab, analysed in this thesis). SWR occur as specific events, not as continuous oscillations (Buzsáki, 2015). SWR comprise ripples viz. high frequency oscillations (110 – 200 Hz) riding on sharp-waves (40 – 100 ms) viz. deflections in the local field potential (LFP, extracellular signal contributed by multiple nearby neurons) (Fig. 2). They can be observed during awake immobility (sitting, grooming, eating, etc.) and non-REM sleep. SWR in area CA1 occur as a result of synchronous firing of neurons; multiple neighbouring neurons are known to fire during SWR events (Buzsáki, 1986). The negative peaks of ripple oscillations correspond to firing of pyramidal neurons – maximum neuronal firing is seen at the negative peaks. On the other hand, the positive peaks of ripple oscillations correspond to the firing of inhibitory neurons (Buzsáki et al., 1992; Ylinen et al., 1995). Additionally, the power of the ripples is correlated with the total activity of the pyramidal neurons during a SWR event (Csicsvari et al, 2000). The synchronous discharge of neurons in area CA1 is believed to be driven mainly by area CA3 as firing of neurons in area CA3 is seen to co-occur with the firing of those in area CA1 during SWR events (Buzsáki et al., 1983; Csicsvari et al., 2000). It has also been observed that lesions to other regions such as the medial septum and the entorhinal cortex do not usually suppress SWR, but in the initial days after entorhinal cortex lesions, increased firing of

multiple neurons and abnormal LFP patterns along with an absence of SWR have been observed (Suzuki and Smith, 1988). However, an increase in the firing of neurons has been observed in the MEC during SWR in the hippocampus (Sullivan et al., 2011). Thus, the occurrence of SWR in CA1 involves a network that comprises CA3 and possibly the entorhinal cortex. SWR are thought to play a role in memory consolidation as disruption of SWR has been shown to impair performance in tasks involving spatial memory (Girardeau et al., 2009).

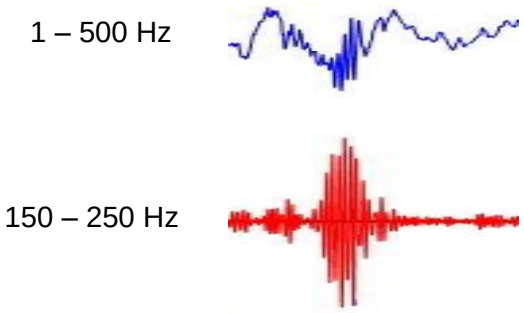

Fig. 2. SWR complex (top) and filtered ripple (bottom) in the LFP of area CA1 (Data collected in Dr. Sachin Deshmukh's lab)

From what we know about SWR, it is evident that they tell us about the activity of hippocampal neurons at the network level. Since SWR occur as events, it is possible to look at differences in the occurrence of these events across the proximal-distal axis. Taking these into consideration along with our observation of differences in occurrence of SWR across the proximal-distal axis of area CA1, SWR are suitable for elucidating the dynamics of the hippocampal-entorhinal network that connects to area CA1 involved in the processing of memories.

We characterised differences in SWR along the proximal-distal axis of area CA1 by analysing SWR recorded during awake immobility and non-REM sleep. Specifically, we characterised the following aspects of SWR:

1. Co-occurrence of SWR across the proximal-distal axis of area CA1 – when SWR occur in one region of CA1, do they co-occur in other regions of CA1.

2. Relative amplitude of ripples across the proximal-distal axis of area CA1 – if SWR co-occur across the proximal-distal axis, are the relative amplitudes of the ripples comparable across the entire axis.
3. Relative time of occurrence of ripple oscillations across the proximal-distal axis – if SWR co-occur across the proximal-distal axis, are the ripples coincident or is there any time lag between the ripples across the proximal-distal axis.

From our understanding of the networks that connect to area CA1, and also from our anecdotal observations of SWR across the proximal-distal axis of area CA1, we expect to see a reduction in co-occurrence as well as relative amplitude, and an increasing time lag as we go from a given region of area CA1 to the other regions.

METHODS

Two adult male Long Evans rats were used for the study. Animal care, surgical procedures, and euthanasia were performed in accordance with the National Institutes of Health (NIH) animal use guidelines and were approved by the Johns Hopkins University Animal Care and Use Committee. The data were collected by Dr. Sachin Deshmukh in the laboratory of Dr. James J. Knierim at the Johns Hopkins University.

Recordings

Rats were chronically implanted with hyperdrives consisting of fifteen tetrodes and two reference tetrodes, which together spanned the entire proximal-distal axis of area CA1 of the right dorsal hippocampus. *In vivo* extracellular recordings of hippocampal LFPs were done from the pyramidal layer of the hippocampus using the Cheetah Data Acquisition system (Neuralynx, Bozeman, MT). One channel from each of the tetrodes were used as the source of LFPs. For this, a 2000-fold amplification of the signals was done. The signals were filtered between 1 and 475 Hz, digitised at 1 kHz, and stored continuously on the PC. Sessions of awake immobility and sleep known as ‘sleep/immobility sessions’ were recorded while the rats were placed on a pedestal. These sleep/immobility sessions were recorded before (session 1) and after (session 2) experimental sessions wherein the rats were allowed to run on a circular track.

Data Analysis

DATA CONSIDERED FOR ANALYSIS

Only LFP recordings from those tetrodes that were positioned in area CA1 were considered for analysis.

Any tetrodes that showed large amounts of noise throughout the length of the signal were eliminated from the analysis before analysing the data. If a relatively large portion of the signal (of the order of minutes) showed large amounts of noise, that portion was eliminated from all tetrodes before the analysis was conducted. If the signal was shortened to less than 10 minutes after such elimination, that data set was not analysed.

Epochs of mobility and REM sleep, characterised by theta oscillations (6 – 10 Hz), were removed from all tetrodes prior to analysing the data. Theta epochs were detected by computing the ratio of the power of the signal in the theta frequency domain (6 – 10 Hz) to that in the supratheta frequency domain (12 – 50 Hz) and considering only those epochs as theta epochs for which the ratio is greater than 0.2 standard deviations below the mean and were greater than 1 s in duration. Power of the signal with respect to time and frequency have been calculated using the multitaper FFT (Mitra and Pesaran, 1999) with a sliding window of length 1 s.

Any tetrodes that were found to be outliers during the initial stage of analysis were removed from further stages of analysis.

RIPPLE DETECTION

Ripples were detected using a thresholding algorithm (Eschenko et al., 2008). The wideband LFP signal (1 – 475 Hz) was first bandpass filtered between 150 Hz and 250 Hz using an IIR filter; the IIR filter was chosen over the FIR filter mainly because it takes less computational time, and it served our purpose. The root mean square (RMS), using a 10 ms window, of the filtered signal was calculated, and a threshold of 6 standard deviations above the mean is used to detect the ripple peak. The beginning and end of a

ripple event were marked by those points at which the RMS fell lower than 1 standard deviation above the mean, and only those events for which the two time points were between 25 ms and 200 ms apart were considered as ripple events. The threshold for RMS chosen for detection of SWR was optimised for minimising the detection of noise events (false-positives optimised to 5 – 10%) as far as possible while not missing out on too many SWR events (false-negatives optimised to ~10%). Noise events were detected visually as those events that were of relatively low amplitude, short duration, and repeating regularly (chewing artefacts, as observed online during recordings), those that were of short duration and relatively low amplitude and those events whose amplitude peaked sharply and were of relatively short duration (seen when the drive hit a surface while the rat was grooming, as observed during online recordings). The fraction of detected events that were noise events was defined as the percentage of false positives. False negatives were also visually detected as those SWR events that were not detected by the thresholding algorithm, and the fraction of all real events (total detected – false positives + false negatives) was defined as the percentage of false negatives.

The efficiency and accuracy of the aforementioned method (Eschenko et al., 2008) were measured and compared to another method used for ripple detection (Karlsson and Frank, 2009). This method employs the Hilbert transform to compute the envelope of the signal, and a thresholding algorithm is used to detect ripples as in the above method. The number of false-positives and false-negatives were comparable for the two methods with optimised thresholds. The two algorithms were also equally efficient in terms of the amount of computational time taken by them. We chose to use the method that uses RMS as it served our purpose.

Since ripples are associated with sharp-waves, we used the presence of ripples as an indicator of the presence of SWR complexes.

DETECTION OF CO-OCCURRENCE OF SWR

To check for co-occurrence of SWR across the proximal-distal axis, the presence of SWR was detected on a tetrode conditional to the presence of SWR on a given reference

tetrode. Such a detection of conditional presence was done for all possible pairs of tetrodes. SWR were considered to co-occur on a referred tetrode with respect to the reference tetrode if there was an overlap between the time window of the ripple on the given tetrode and that on the reference tetrode, the time window of the ripple being defined by the start and end times of the ripple.

While doing the conditional presence detection, it was noticed that some low amplitude ripples on the referred tetrode that co-occurred with ripples on the reference tetrode were not being detected. Therefore, if there was no ripple event detected on the referred tetrode when there was an event present on the reference tetrode, the threshold for ripple peak detection was lowered to 2 standard deviations, while that for ripple boundary detection was kept unchanged at 1 standard deviation. If no ripple was detected despite this lower threshold, no further lowering of the threshold was done, and the ripple was considered as absent.

MEASUREMENT OF RELATIVE RIPPLE AMPLITUDE

Ripple amplitude was measured in a manner similar to how co-occurrence of ripples was detected. Whenever there was a ripple detected on the reference tetrode (using only the 6 standard deviation threshold), the peak amplitude of the ripple on the reference tetrode, as well as the corresponding peak amplitudes on the other tetrodes were measured. This amplitude measurement was done irrespective of the co-occurrence of ripples on the tetrodes. The time window within which the peak amplitude was measured was defined by the boundaries of the ripple on the referred tetrode if there was a co-occurring ripple on the referred tetrode with respect to the reference tetrode. If there was no ripple co-occurring on the referred tetrode, the time window was defined by the boundaries of the ripple on the reference tetrode.

In order to account for the possible differences in gains of the tetrodes, amplitudes measured on each tetrode were normalised by that of the ripple having the maximum amplitude on the respective tetrode.

MEASUREMENT OF RIPPLE PEAK TIME

The time at which a ripple event occurred was defined by the time at which the amplitude of the ripple was maximum. The envelope of the signal was calculated using the analytical signal, and then smoothed using a Gaussian of 4 ms standard deviation (Karlsson and Frank, 2009). The time of the peak amplitude was then determined as the time corresponding to the maximum of the envelope within a given ripple's boundaries.

To look at differences in the time of ripples co-occurring across the proximal-distal axis, the difference between the times of peak amplitudes was calculated for any given tetrode with respect to a reference tetrode (referred tetrode peak time – reference tetrode peak time).

STATISTICAL ANALYSIS

For looking at trends in the analysed data across the proximal-distal axis, lines were fitted using linear regression analysis. Lines were fitted for data points on either side of the reference tetrode. Thus, for the reference tetrodes at the two extremes, a single line was fitted, while for those with more than two data points on either side of the reference tetrode, two lines were fitted. Goodness of fit was measured using co-efficient of determination (r^2). Significance was checked using an alpha value of 0.05 using Holm Bonferroni correction for multiple comparisons. For this quantitative analysis, only the proximal-most and distal-most reference tetrode were used from session 1 of day 1 for both rats.

Histology and measurement of relative distances between tetrodes

A current of 10 μA was passed for 10 s in order to create marker lesions on a subset of the tetrode tips at the end of the experiment. A freezing microtome was used to cut sections (40 μm coronal), which were then mounted and stained with 0.1% cresyl violet. Tetrode tracks were then reconstructed, and the position of a tetrode in the hippocampus was defined by the end point of the tetrode track. Positions of tetrodes along the medio-lateral (ML) axis were measured as the lengths of the positions of the tetrodes from the midline, and positions along the anterio-posterior (AP) axis were measured by counting the number of 40 μm slices from the anterior side of the brain till the positions of the

tetrodes. The hyperdrive was angled at 35° to the ML axis. To calculate the position of the tetrodes along the long axis of the hyperdrive, a counter-clockwise rotation of the ML-AP co-ordinate system by 35° was done using the following formula:

$$\text{long axis position} = (\text{ML axis position}) \times \cos(35°) + (\text{AP axis position}) \times \sin(35°)$$

To calculate the distance of all tetrodes with reference to the proximal-most tetrode, positions determined in this manner were subtracted from the position of the proximal-most tetrode. Thus, the distance of the proximal-most tetrode was 0 mm, and the distances of the subsequent tetrodes were finite positive values.

Tetrodes were labelled as either ‘P’ (proximal), ‘I’ (intermediate), or ‘D’ (distal) depending on the region in which they were positioned in area CA1 along with a number depending on how they were ordered in their respective region in terms of their distance from the proximal-most tetrode. For example, the proximal-most tetrode is ‘P1’, the intermediate tetrode closest to proximal CA1 is ‘I1’, while the next-closest intermediate tetrode is ‘I2’.

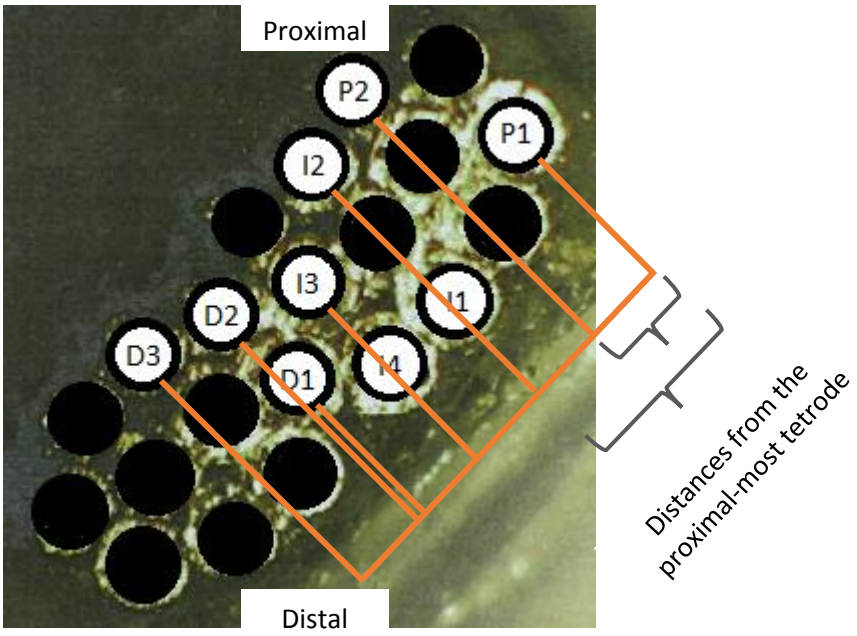

Fig. 3. Top view of the hyperdrive of rat 432. Darkened circles indicate either no tetrode in that position or a tetrode not used for the analysis

RESULTS

We observed differences in the nature of occurrence of SWR across the proximal-distal axis of area CA1 of the hippocampus during neural recordings. To confirm our observations, we characterised differences in co-occurrence, relative amplitudes, and time of occurrence of SWR across the proximal-distal axis of area CA1.

1. Rate of SWR occurrence across the proximal-distal axis is similar

Rate of SWR occurrence on any given tetrode was measured as the number of events that occurred on the given tetrode over the entire time for which recordings were performed divided by the total time for which the recording was performed.

For both rats, the rate was similar, and fell in the range of 15-20 SWR per minute (Fig. 4). We did not check for statistical significance of difference in rates between tetrodes as we had single data points for each tetrode in both rats. Thus, the rate of occurrence of SWR across the proximal-distal axis of area CA1 is similar.

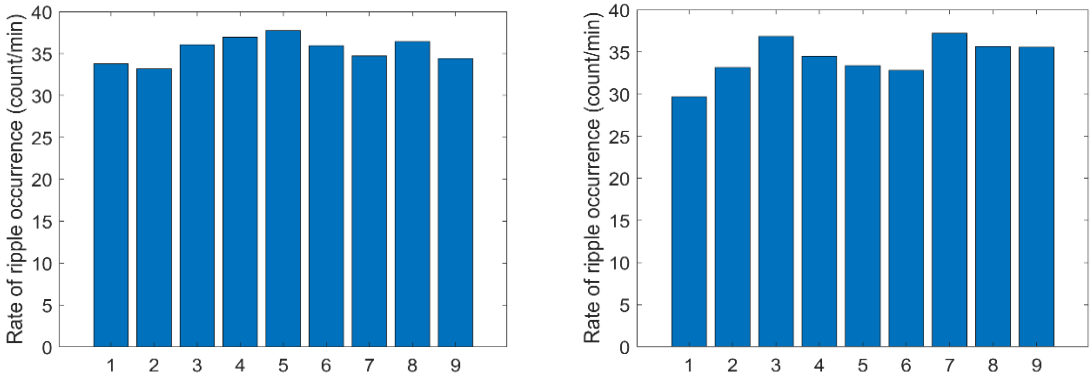

Fig. 4. Rate of SWR occurrence for a) rat 432 and b) rat 441

2. Probability of co-occurrence of SWR reduces as a function of distance from the reference tetrode

Having seen that the number of SWR across the proximal-distal axis were similar in a given duration of time, we went on to look at whether these events co-occur across the proximal-distal axis, or whether SWR on one tetrode might occur independently of those on another tetrode.

SWR on a referred tetrode that co-occurred with SWR on a given reference tetrode were detected. The conditional probability of a SWR occurring on a referred tetrode given that a SWR occurred on the reference tetrode was computed by calculating the fraction of co-occurring SWR on the referred tetrode with respect to the reference tetrode. This conditional probability of co-occurrence was calculated using each tetrode as a reference.

The conditional probability of a SWR occurring with respect to the reference tetrode reduced with an increase in distance from the reference tetrode (Fig. 3, Fig. 5). Although the range of conditional probability across the proximal-distal axis was not large ($0.7 <$ conditional probability < 1), there was a significant trend (with correction for multiple comparisons) in the probability for rat 432 (proximal-most reference: $p = 0.0034$, $r^2 = 0.78$, distal-most reference: $p = 0.0011$, $r^2 = 0.85$) (Fig. 4(a)) as well as rat 441 (proximal-most reference: $p = 0.0026$, $r^2 = 0.8$, distal-most reference: $p = 0.0035$, $r^2 = 0.78$) (Fig. 6(a)). The trend was observed across sleep sessions (before and after behaviour sessions), and also over days in both rats (Fig 4, Fig. 6). The data from these different sessions across days were repeat observations recorded from the same tetrodes which had not been moved from the pyramidal layer. Hence, these data have been displayed for descriptive purposes; we have not performed any quantitative analysis on them. Thus, SWR are more likely to co-occur on tetrodes close to the reference and relatively less likely to co-occur on tetrodes that are further away in area CA1, and this seems to be independent of the position of the reference tetrode.

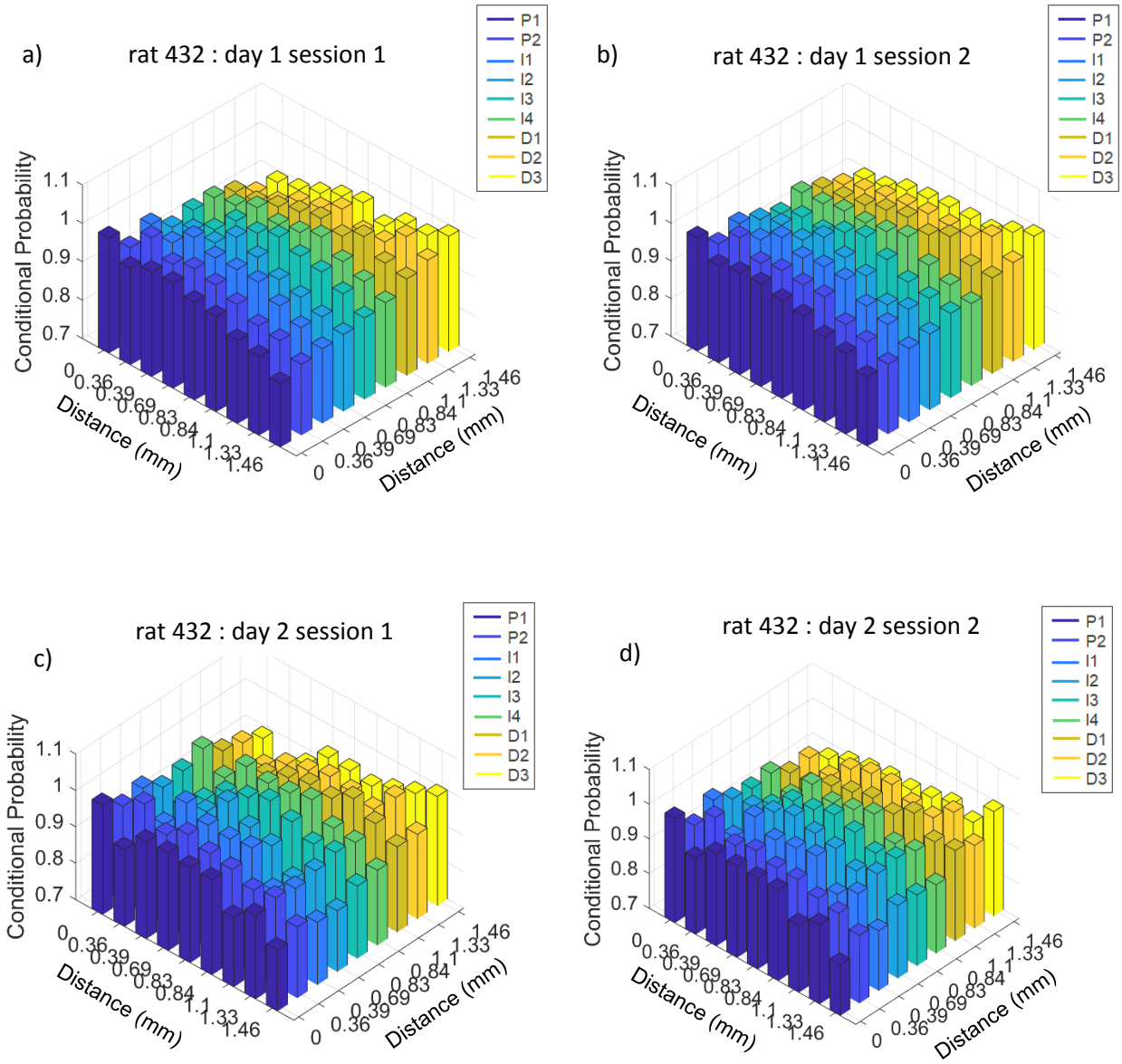

Fig. 5. Conditional probability of co-occurrence of SWR across the proximal-distal axis of CA1 for rat 432. Bars of the same colour correspond to conditional probability computed with respect to the same reference tetrode. Distances on the x-axis are the distances of the reference tetrode from the proximal-most tetrode, while those on the y-axis are the distance of the referred tetrode from the proximal-most tetrode. Plots have been shown for the two different sessions across days.

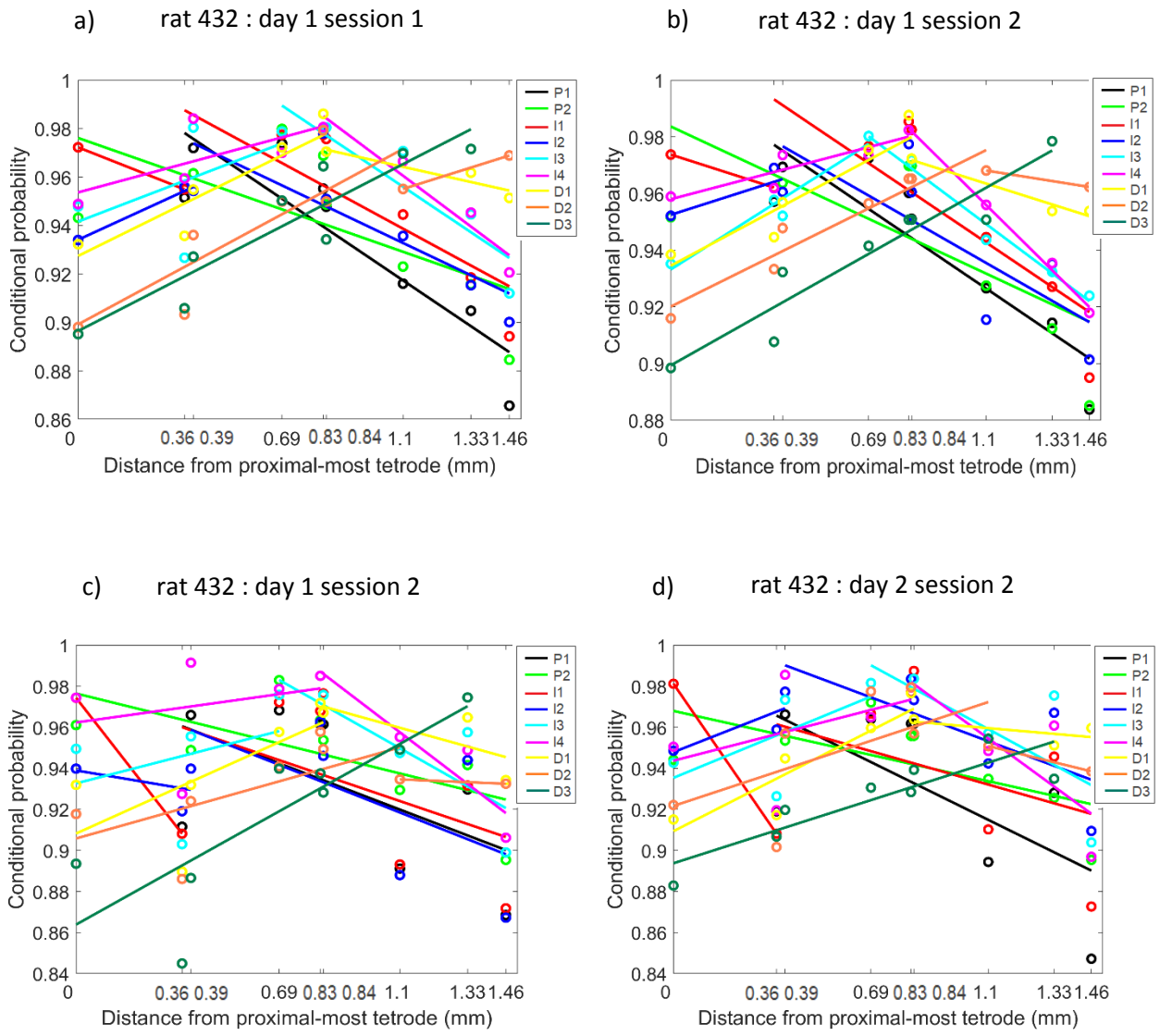

Fig. 6. Conditional probability of co-occurrence of SWR across the proximal-distal axis of CA1 for rat 432 along with regression analysis. Lines were fitted for data points on either side of the reference tetrode. Lines of the same colour correspond to conditional probability computed with respect to the same reference tetrode. Plots have been shown for the two different sessions across days.

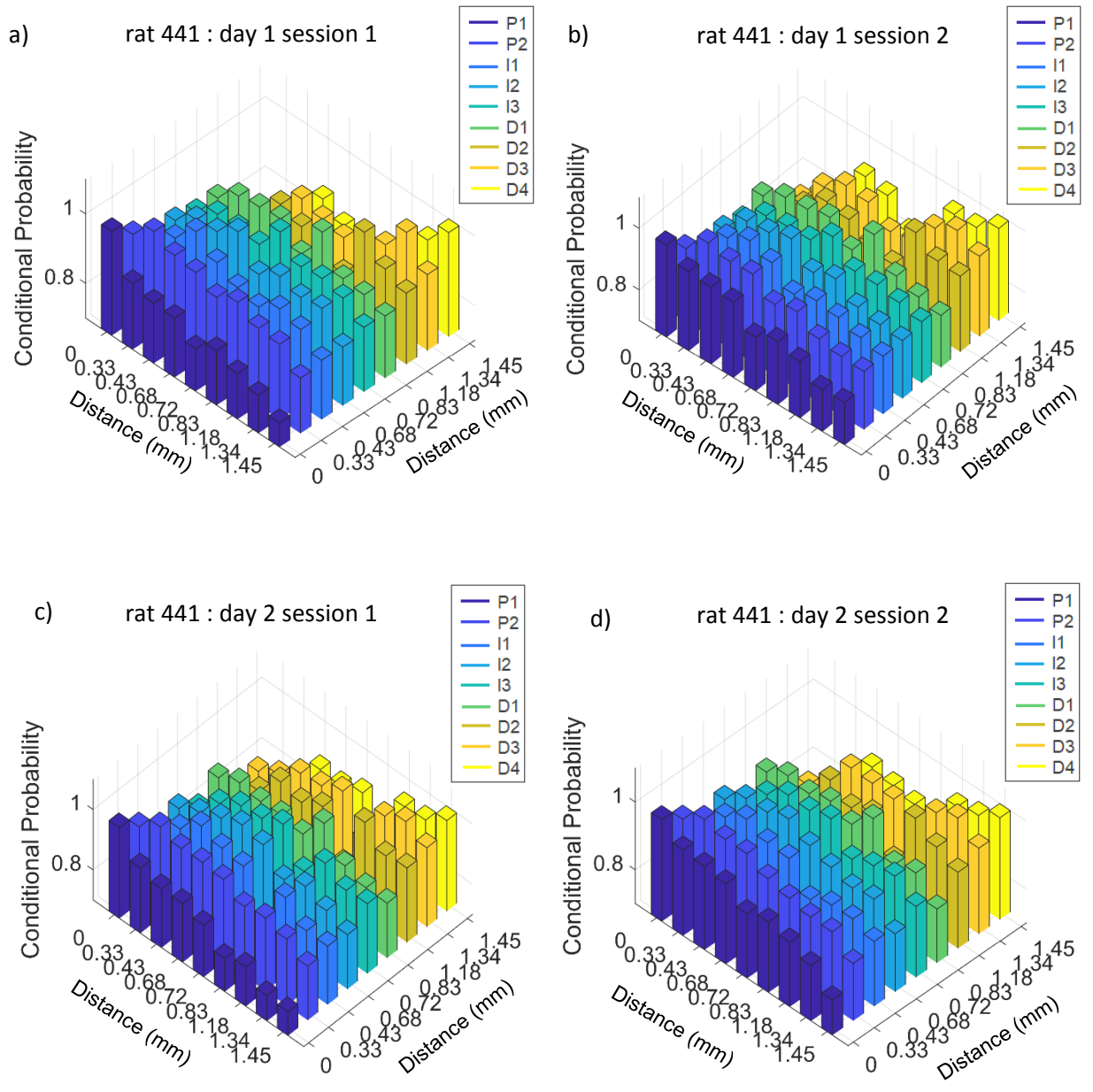

Fig. 7. Conditional probability of co-occurrence of SWR across the proximal-distal axis of CA1 for rat 441. Bars of the same colour correspond to conditional probability computed with respect to the same reference tetrode. Distances on the x-axis are the distances of the reference tetrode from the proximal-most tetrode, while those on the y-axis are the distance of the referred tetrode from the proximal-most tetrode. Plots have been shown for the two different sessions across days.

a) rat 441 : day 1 session 1

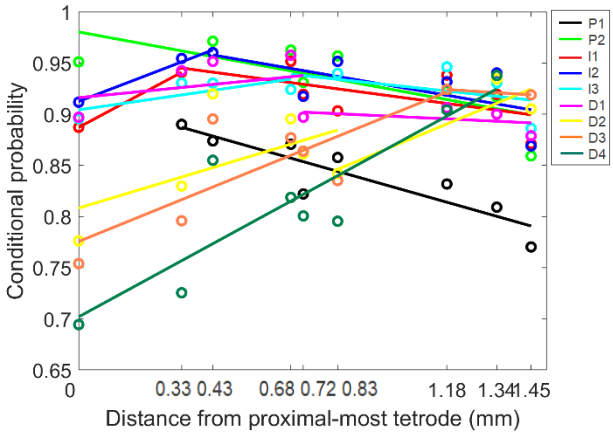

b) rat 441 : day 1 session 2

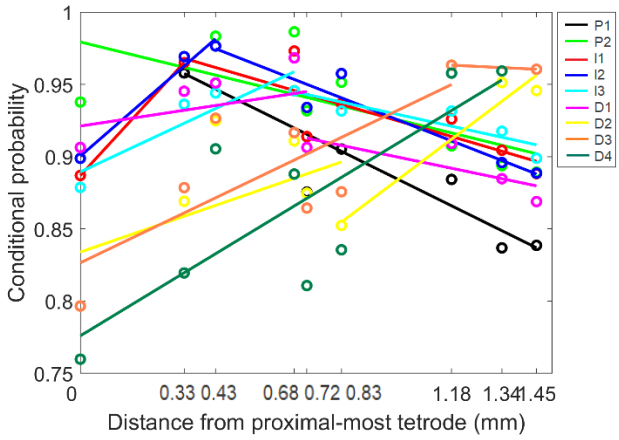

c) rat 441 : day 2 session 1

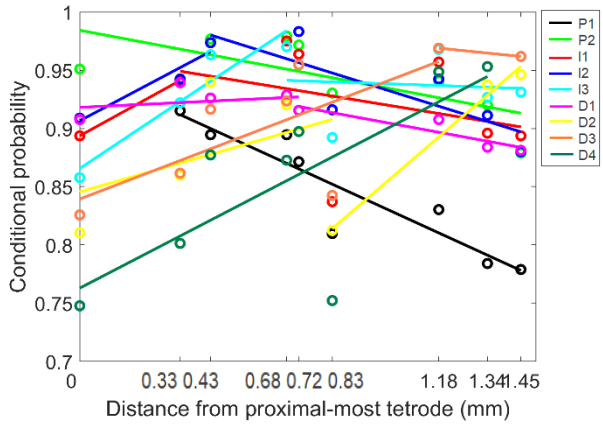

d) rat 441 : day 2 session 2

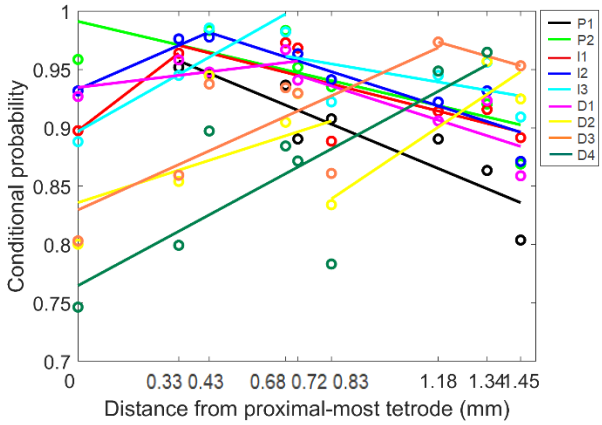

Fig. 8. Conditional probability of co-occurrence of SWR across the proximal-distal axis of CA1 for rat 441 along with regression analysis. Lines were fitted for data points on either side of the reference tetrode. Lines of the same colour correspond to conditional probability computed with respect to the same reference tetrode. Plots have been shown for the two different sessions across days.

Since the decrease in probability of co-occurrence seemed to depend only on the distance of the referred tetrode from the reference tetrode, we looked at probability of co-occurrence as a function of distance between pairs of tetrodes (relative distance) wherein one tetrode was a reference, and the other was the referred. If the reference was more distal to the referred tetrode, the distance was taken as negative, and if the reference was more proximal to the referred tetrode, distance was taken as positive. Data from all sessions for a given rat were pooled, and the data for each relative distance from both rats was analysed collectively.

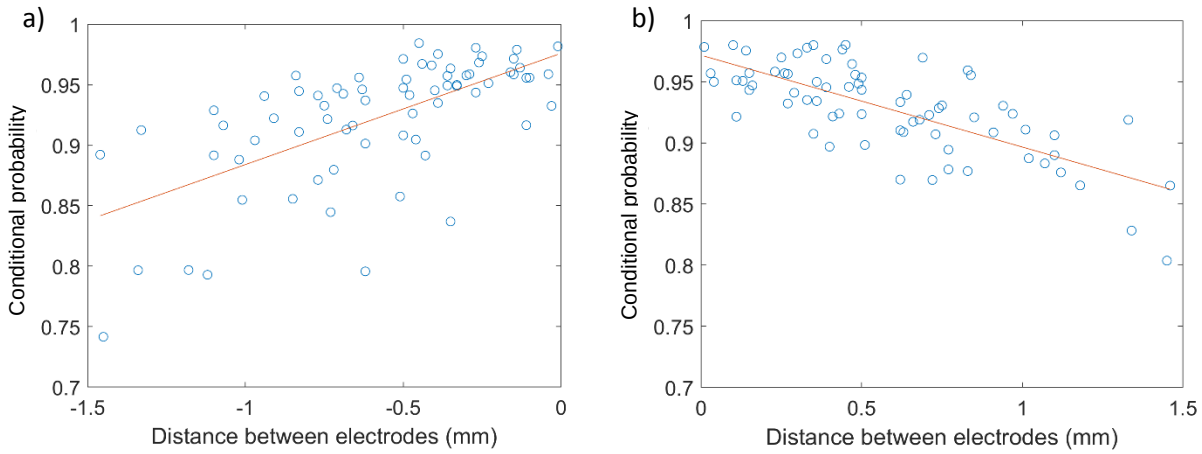

Fig. 9. Conditional probability of co-occurrence of SWR across the proximal-distal axis of area CA1 as a function of distance between pairs of tetrodes.
a) Plot for pairs of tetrodes with the reference tetrode more distal to the referred tetrode.
b) Plot for pairs of tetrodes with the reference tetrode more proximal to the referred tetrode.

This analysis yielded significant trends in probability of co-occurrence (using correction for multiple comparisons) (plot (a): $p = 1.39 \times 10^{-9}$, $r^2 = 0.41$; plot (b): $p = 3.49 \times 10^{-13}$, $r^2 = 0.53$). Thus, the probability of co-occurrence of SWR decreases as a function of distance between tetrodes.

3. Relative amplitude of ripples reduces as a function of distance from the reference tetrode

The detection of co-occurring SWR required more than one threshold to successfully detect ripples of relatively low amplitudes on any tetrode that co-occurred with ripples on the reference tetrode (as mentioned in Methods). Hence, we looked at how the amplitudes of ripples might vary across the proximal-distal axis.

With respect to the ripples that occurred on a given reference tetrode, corresponding peak amplitudes were measured on all other tetrodes. Amplitudes measured in this manner on the referred tetrodes were first normalised with respect to the maximum ripple amplitude on the respective referred tetrode. Next, the ratio of the normalised ripple amplitude on a referred tetrode to the corresponding normalised ripple amplitude on the reference tetrode were calculated. We then looked at the distribution of these relative amplitudes with respect to each reference tetrode.

The peaks of the distributions were observed to shift to the left of 1 as one went from the reference tetrode to tetrodes further away (Fig. 7(a), Fig. 9(a)). To confirm this observed trend, trends in the medians of these distributions were looked at. Median was chosen over mean as the distributions were skewed. This analysis yielded trends similar to those seen in simultaneous occurrence of SWR i.e. relative amplitude reduced as a function of distance from the reference tetrode (Fig. 7(b), Fig. 9(b)). These trends (with correction for multiple comparisons), however, were not significant for rat 432 (proximal-most reference: $p = 0.0451$, $r^2 = 0.51$, distal-most reference: $p = 0.056$, $r^2 = 0.48$) (Fig. 7(b)) and significant for the distal-most tetrode in rat 441 (proximal-most reference: $p = 0.36$, $r^2 = 0.13$, distal-most reference: $p = 0.0068$, $r^2 = 0.73$) (Fig. 9(b)). The observed trends were seen in most sessions across other days (Fig. 8, Fig. 10). This observed trend could imply that when a ripple was detected in one region of area CA1, it was of relatively high amplitude, and the relative amplitude progressively reduced with an increase in distance from that region. The trends may not have been significant due to the sample size not being sufficiently large. To account for this, the data from across sessions and days can be pooled.

rat 432 : day 1 session 1

a)

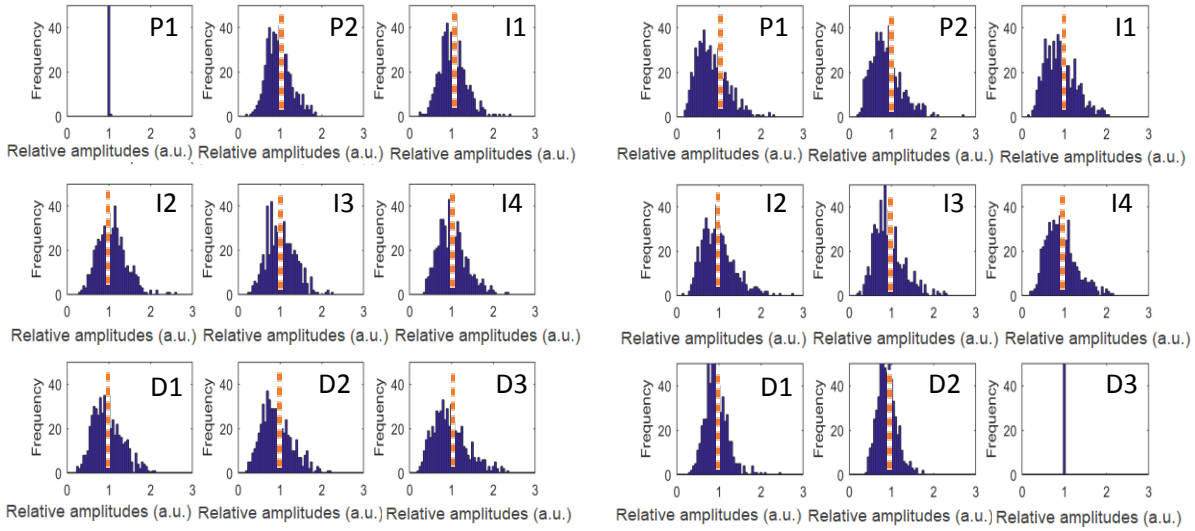

b)

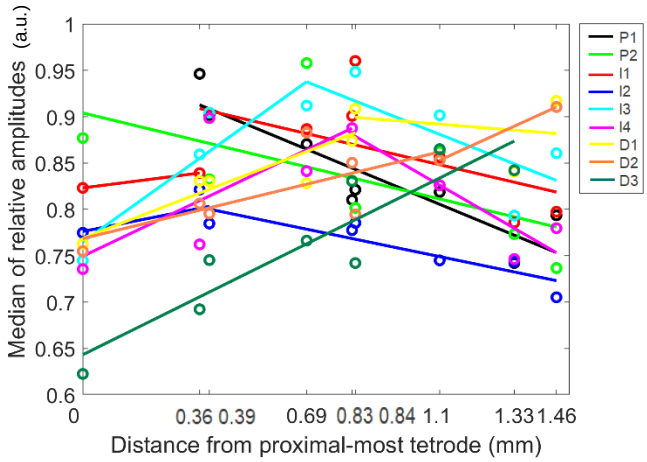

Fig. 10. Ratio of relative amplitudes between referred tetrodes and reference tetrodes for rat 432.

a) Distributions of ratios of relative amplitudes for each referred tetrode with respect to the proximal-most tetrode (left) and distal-most tetrode (right).

b) Medians of the distributions with regression analysis for each reference tetrode plotted as a function of distance; lines were fitted for data points on either side of the reference tetrode (each colour corresponds to a single reference tetrode).

a) rat 432 : day 1 session 2

b) rat 432 : day 2 session 1

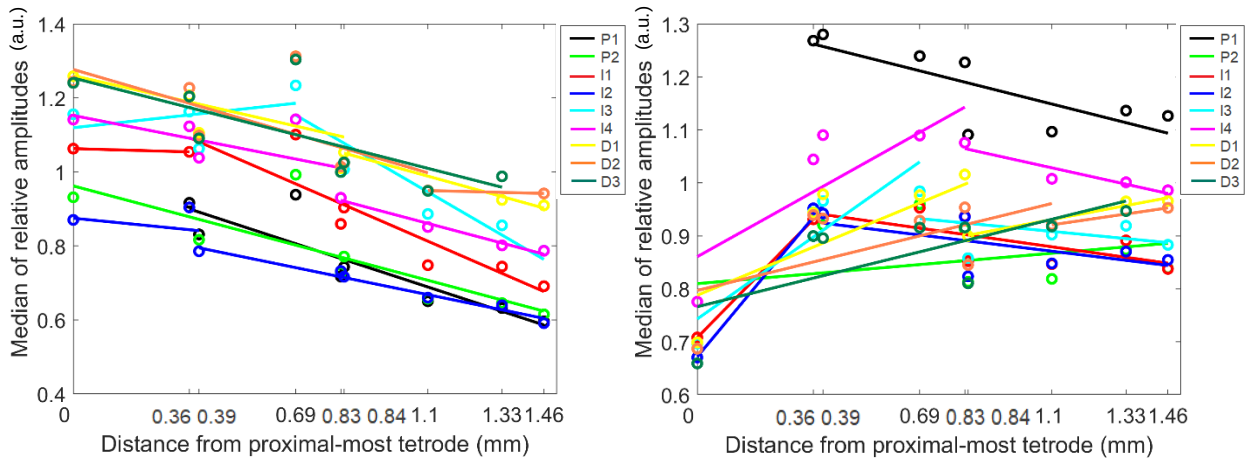

c) rat 432 : day 2 session 2

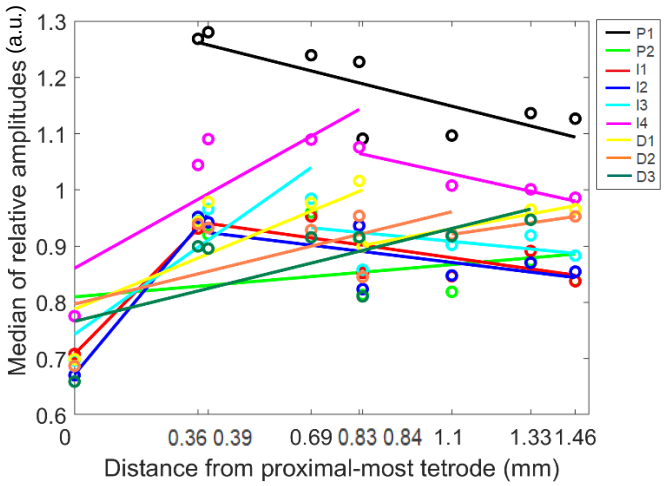

Fig. 11. Ratio of relative amplitudes between referred tetrodes and reference tetrodes for rat 432 for the different sessions across days. Medians of the distributions with regression analysis for each reference tetrode plotted as a function of distance; lines were fitted for data points on either side of the reference tetrode (each colour corresponds to a single reference tetrode) for all ripple events.

rat 441 : day 1 session 1

a)

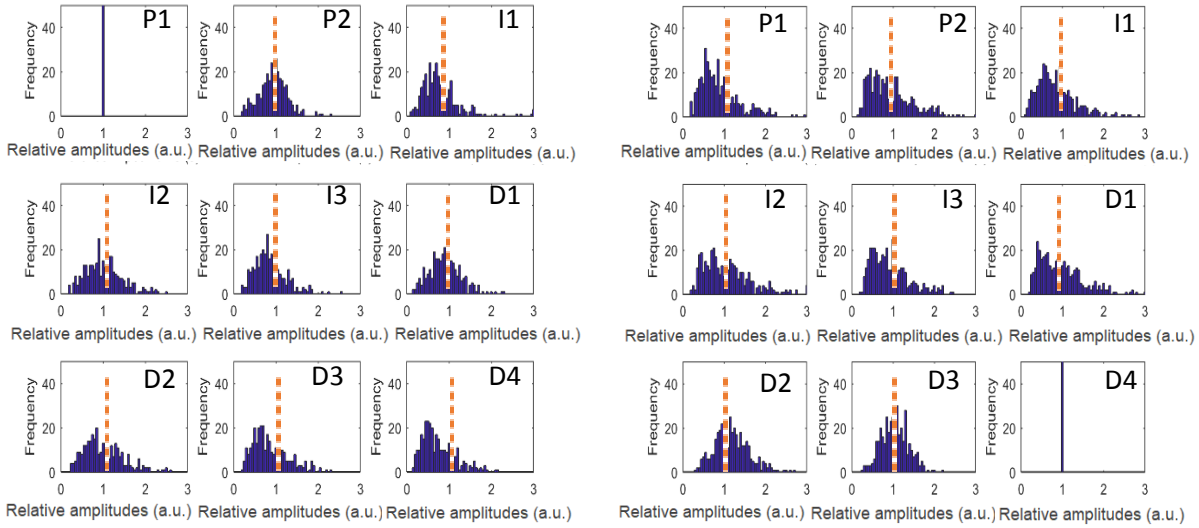

b)

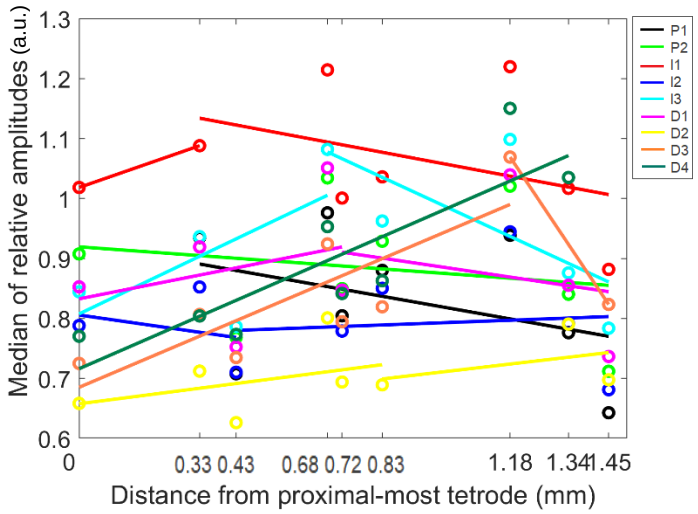

Fig. 12. Ratio of relative amplitudes between referred tetrodes and reference tetrodes for rat 441.

a) Distributions of ratios of relative amplitudes for each referred tetrode with respect to the proximal-most tetrode (left) and distal-most tetrode (right).

b) Medians of the distributions with regression analysis for each reference tetrode plotted as a function of distance; lines were fitted for data points on either side of the reference tetrode (each colour corresponds to a single reference tetrode).

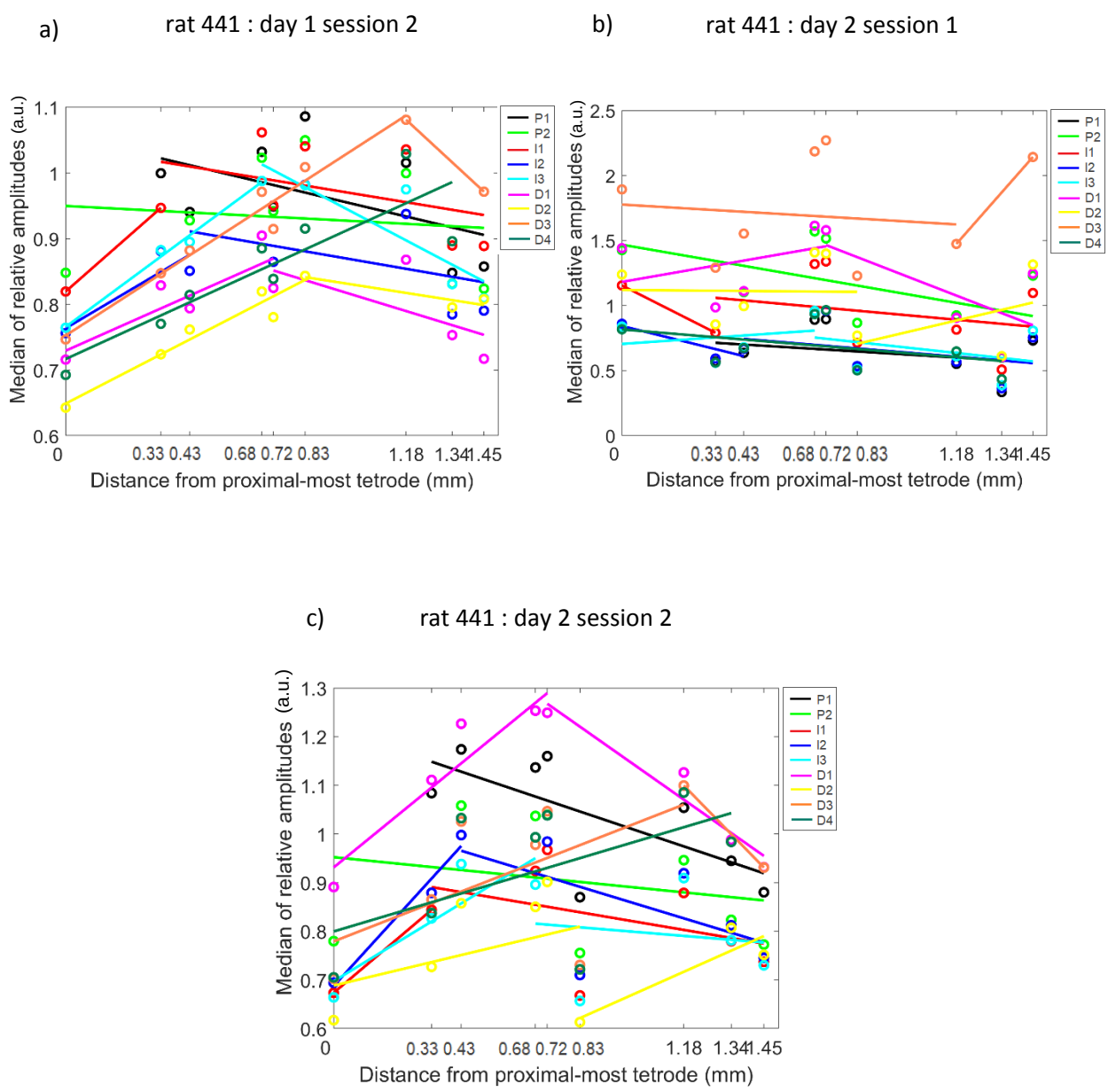

Fig. 13. Ratio of relative amplitudes between referred tetrodes and reference tetrodes for rat 441 for the different sessions across days. Medians of the distributions with regression analysis for each reference tetrode plotted as a function of distance; lines were fitted for data points on either side of the reference tetrode (each colour corresponds to a single reference tetrode) for all ripple events.

Since the decrease in relative amplitude seemed to depend only on the distance of the referred tetrode from the reference tetrode, we looked at relative amplitude as a function relative distance, just as we did for probability of co-occurrence.

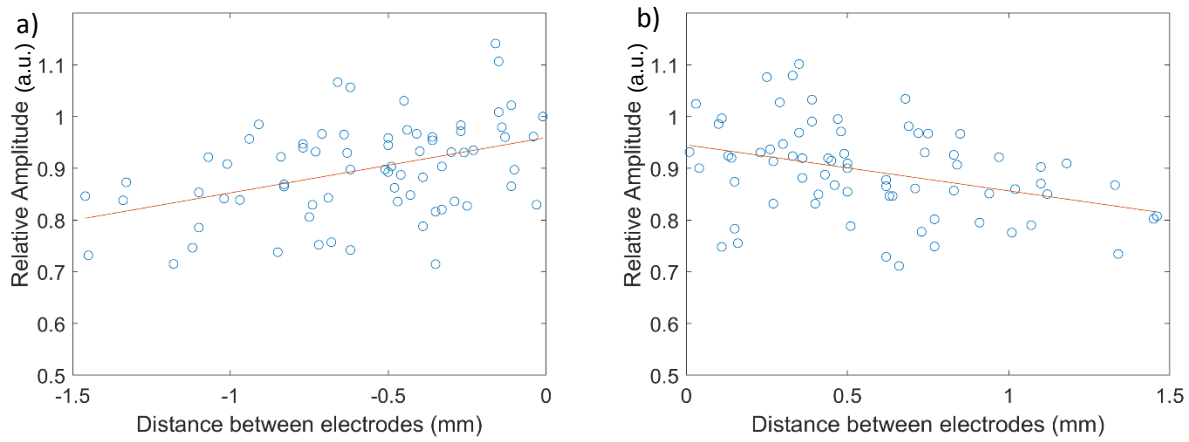

Fig. 14. Relative amplitude of ripples across the proximal-distal axis of area CA1 as a function of distance between pairs of tetrodes.
c) Plot for pairs of tetrodes with the reference tetrode more distal to the referred tetrode.
d) Plot for pairs of tetrodes with the reference tetrode more proximal to the referred tetrode.

This analysis yielded significant trends in relative amplitude (using correction for multiple comparisons) (plot (a): $p = 0.00026$, $r^2 = 0.18$; plot (b): $p = 0.00167$, $r^2 = 0.13$).

To corroborate the trends observed above, the trend in relative amplitudes while specifically considering relatively high amplitude ripples on the reference tetrode was also looked at. Relatively high amplitude ripples on the reference tetrode were selected by taking those ripples whose amplitude fell in the top 30 percentile of the relative ripple amplitude range (0.7 – 1 a.u.). This procedure of selection yielded a low number of ripple events per session per day (at most 50 of the total number of ripple events per tetrode). Therefore, the ripples during both sessions (session 1 and session 2) and on each day that met this criterion were collectively analysed. The peak shift in the relative amplitude distributions with respect to the reference tetrode were more prominent (Fig. 11(a), Fig. 12(a)). Observed trends in medians were similar to those seen in the above analysis but were significant (with correction for multiple comparisons) for rat 432 (proximal-most reference: $p = 0.022$, $r^2 = 0.61$, distal-most reference: $p = 0.00046$, $r^2 = 0.89$) as well as rat 441 (proximal-most reference: $p = 0.031$, $r^2 = 0.57$, distal-most reference: $p = 0.0058$, $r^2 = 0.74$) (Fig. 11(b), Fig. 12(b)).

Thus, it is evident that there is a gradient in the relative amplitudes of ripples along the proximal-distal axis as a function of distance from a given region of area CA1.

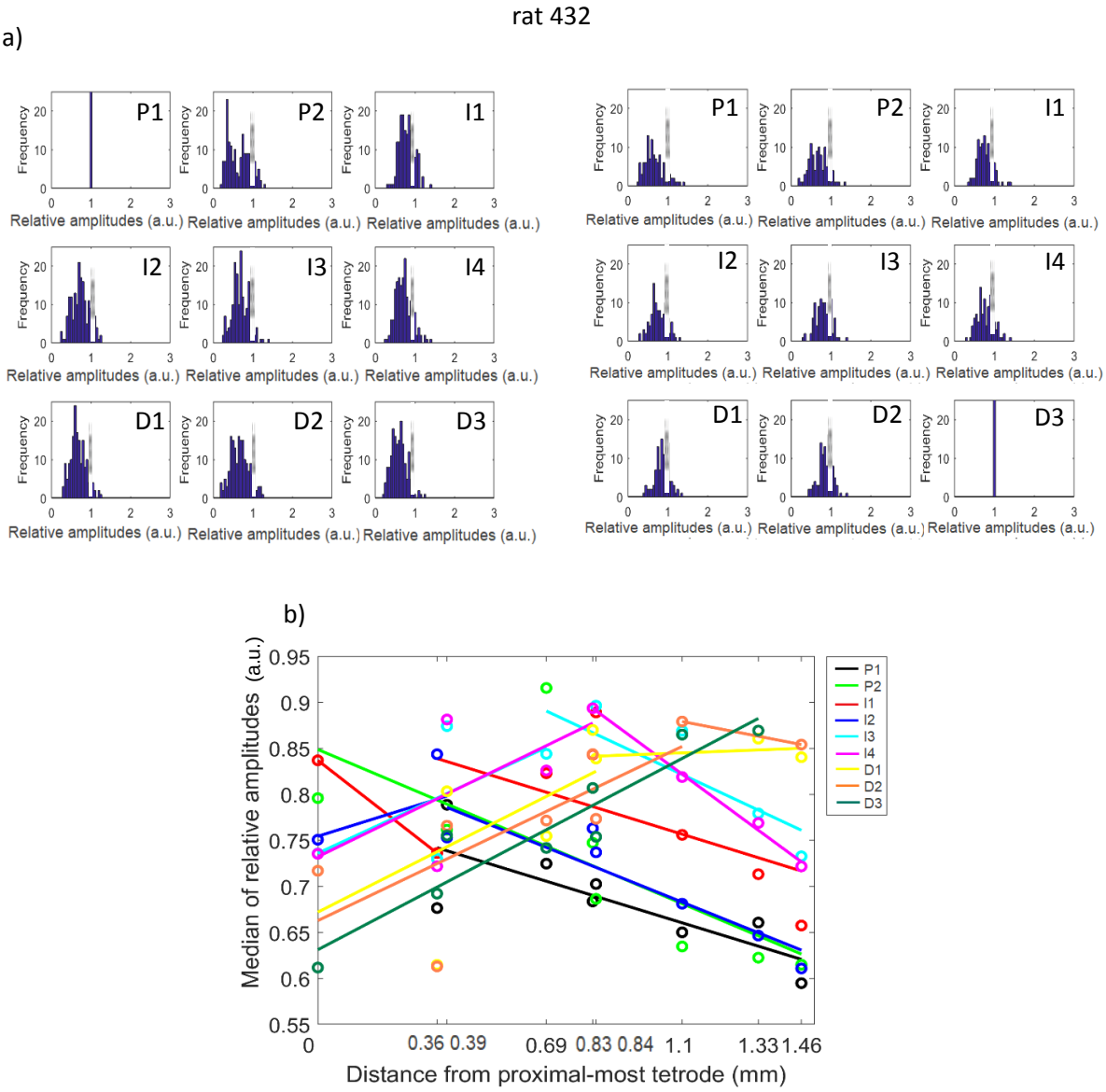

Fig. 15. Ratio of relative amplitudes between referred tetrodes and reference tetrodes taken for the top 30 percentile of relative amplitude values for rat 432.

a) Distributions of ratios of relative amplitudes for each referred tetrode with respect to the proximal-most tetrode (left) and distal-most tetrode (right).

b) Medians of the distributions with regression analysis for each reference tetrode plotted as a function of distance; lines were fitted for data points on either side of the reference tetrode (each colour corresponds to a single reference tetrode).

rat 441

a)

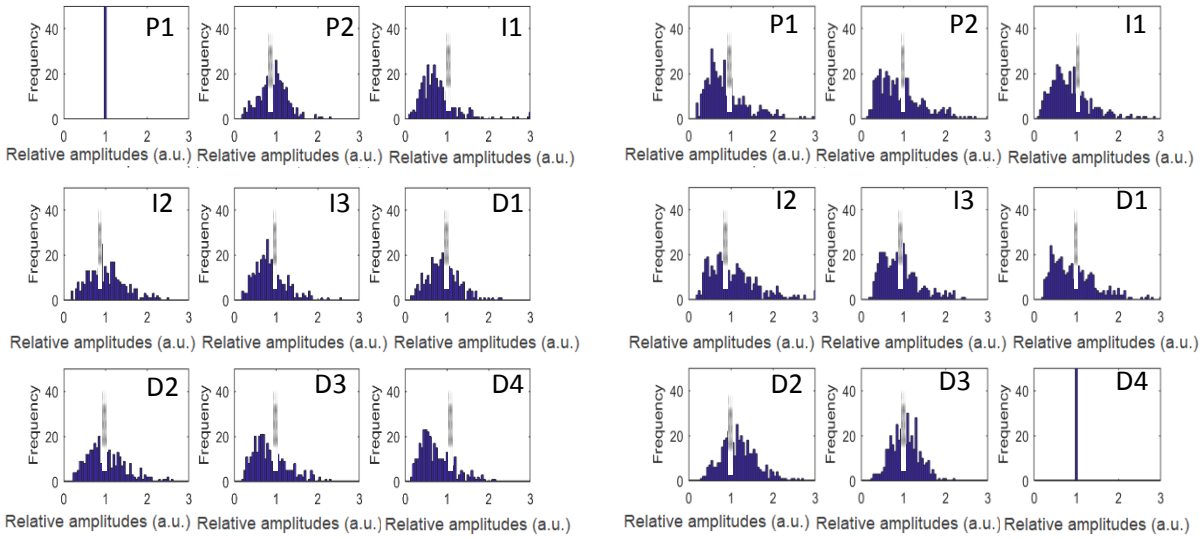

b)

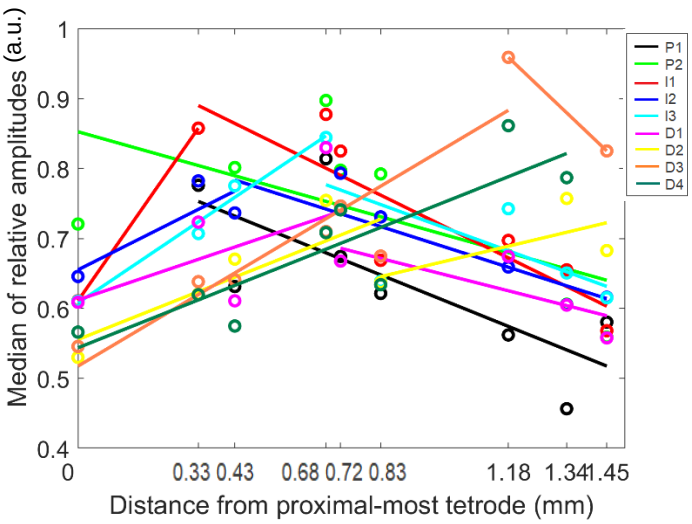

Fig. 16. Ratio of relative amplitudes between referred tetrodes and reference tetrodes taken for the top 30 percentile of relative amplitude values for rat 441.

a) Distributions of ratios of relative amplitudes for each referred tetrode with respect to the proximal-most tetrode (left) and distal-most tetrode (right).

b) Medians of the distributions with regression analysis for each reference tetrode plotted as a function of distance; lines were fitted for data points on either side of the reference tetrode (each colour corresponds to a single reference tetrode).

Since the decrease in relative amplitude seemed to depend only on the distance of the referred tetrode from the reference tetrode in this case too, we once again looked at relative amplitude as a function relative distance.

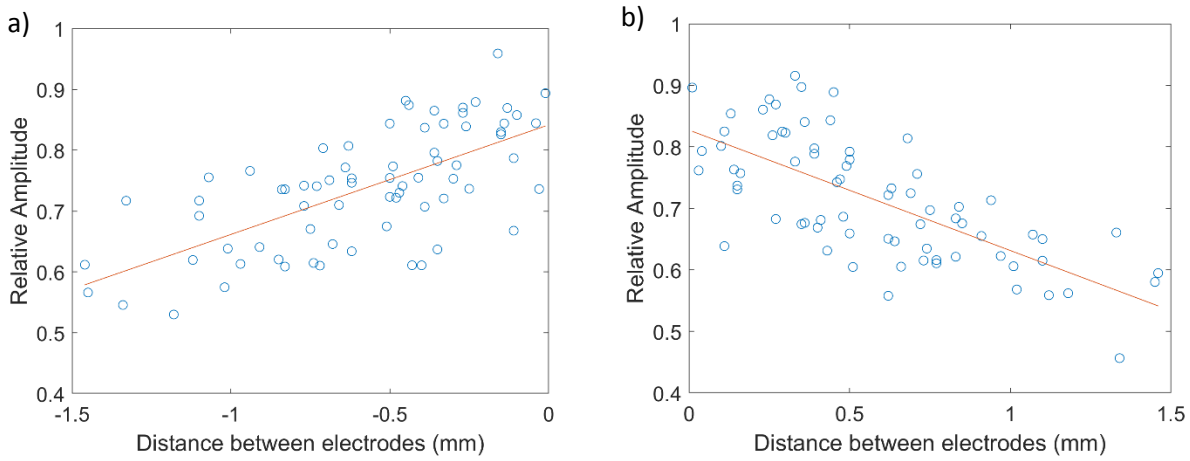

Fig. 17. Relative amplitude of ripples across the proximal-distal axis of area CA1 as a function of distance between pairs of tetrodes taken for the top 30 percentile of relative amplitude values on the reference.
e) Plot for pairs of tetrodes with the reference tetrode more distal to the referred tetrode.
f) Plot for pairs of tetrodes with the reference tetrode more proximal to the referred tetrode.

This yielded significant trends (with corrections for multiple comparisons) (plot (a): $p = 1.18 \times 10^{-10}$, $r^2 = 0.45$; plot (b): $p = 7.03 \times 10^{-12}$, $r^2 = 0.49$) once again. Thus, relative amplitude decreases as a function of distance across the proximal-distal axis. This gradient in amplitudes could possibly explain the gradient in probability of ripple detection seen in the previous section – tetrodes further away from the reference tetrode possibly had a larger fraction of events corresponding to the ripples on the reference tetrode that did not cross the 2 standard deviation threshold.

4. Ripples might occur earlier in distal CA1 than proximal CA1

The gradient in amplitudes across the proximal-distal axis could indicate that SWR are initiated in one region of CA1 and progress to the other regions. To elucidate this possible phenomenon, we looked at the difference in times of the peaks of ripples across the proximal-distal axis.

Differences in ripple peak times were computed for any given tetrode with respect to a reference tetrode (referred tetrode peak time – reference tetrode peak time). Thus, if the difference was positive, the ripple peak on the referred tetrode occurred after the ripple peak on the reference tetrode, while if the difference was negative, the ripple peak on the referred tetrode occurred before the ripple peak on the reference tetrode. Similar to the analysis of amplitudes, we looked at the distribution of these time differences with respect to each reference tetrode.

We did not observe any obvious shifts in the peaks of the distributions of differences in time (Fig. 13(a), Fig. 15(a)). To confirm this, trends in the means of these distributions were looked at. The means did show trends – the time difference for ripples on tetrodes proximal to the reference tetrode were usually positive while that for ripples distal to the reference tetrode were usually negative.

Since our data was acquired at 1 kHz, any differences in peak times could only be multiples of 1 ms. However, means yielded continuous values rather than discrete values as a result of averaging. Hence, we looked at median values to account for this. The medians did not always capture the trend though (significance was tested with correction for multiple comparisons) (proximal-most reference: $p = 0.66$, $r^2 = 0.034$, distal-most reference: $p = 0.007$, $r^2 = 0.73$) (Fig. 13(c)) while the means did (proximal-most reference: $p = 0.0354$, $r^2 = 0.55$, distal-most reference: $p = 0.00086$, $r^2 = 0.86$) (Fig. 13(b)). We, therefore, continued to use the mean of the distributions for the analysis, and only looked at trends in the data; we did not infer anything regarding the actual differences in peak times. The observed trend followed by the means was mostly consistent across different

sessions and days, for the two rats (Fig. 14, Fig. 16). Thus, ripples might occur relatively earlier in the distal region than the proximal region of area CA1.

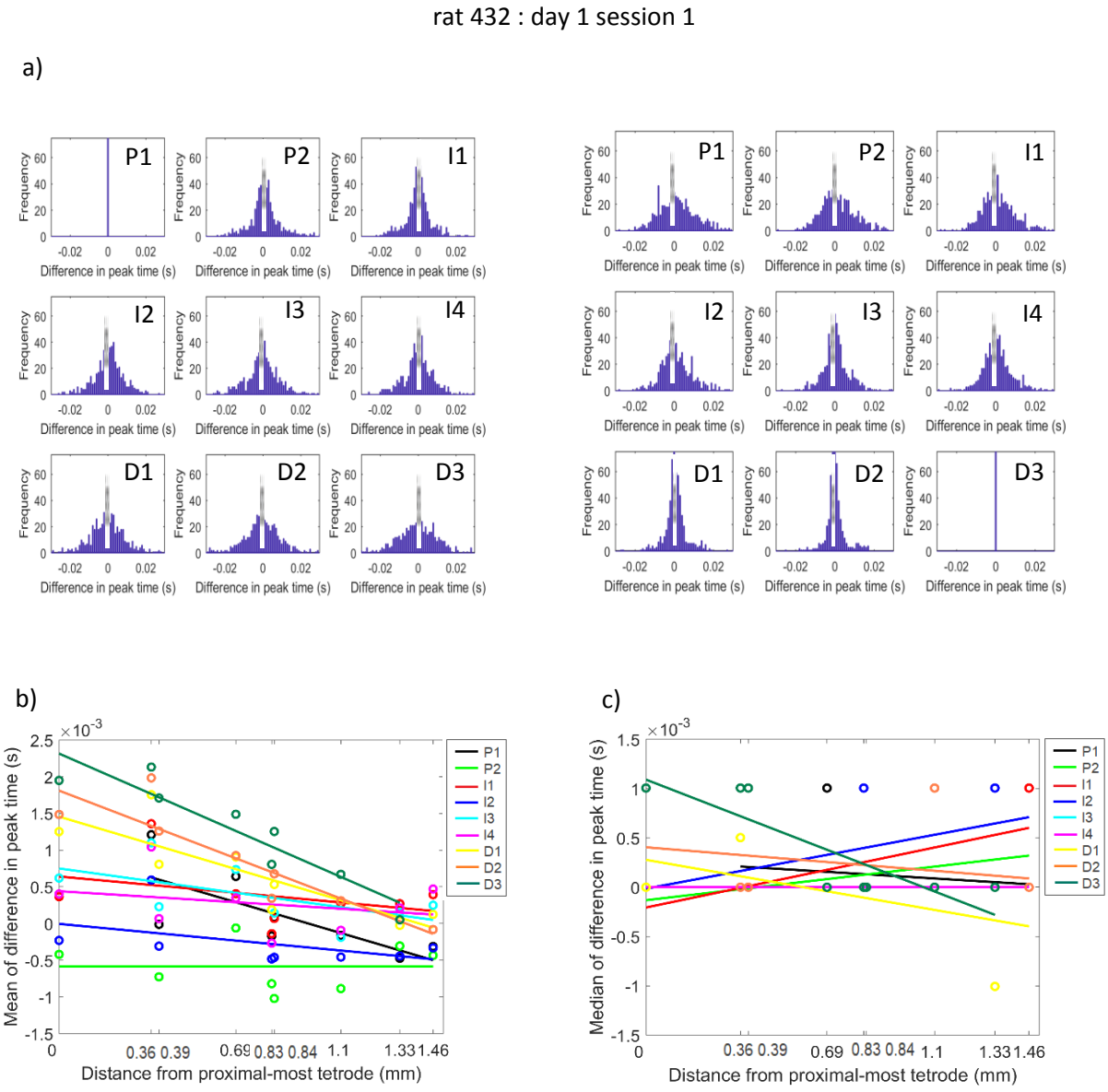

Fig. 18. Differences in peak time between referred tetrodes and reference tetrodes for rat 432.

a) Distributions of differences in peak time for each referred tetrode with respect to the proximal-most tetrode (left) and distal-most tetrode (right).

b) Means of the distributions with regression analysis for each reference tetrode plotted as a function of distance (each colour corresponds to a single reference tetrode).

c) Medians of the distributions with regression analysis for each reference tetrode plotted as a function of distance (each colour corresponds to a single reference tetrode).

a) rat 432 : day 1 session 2

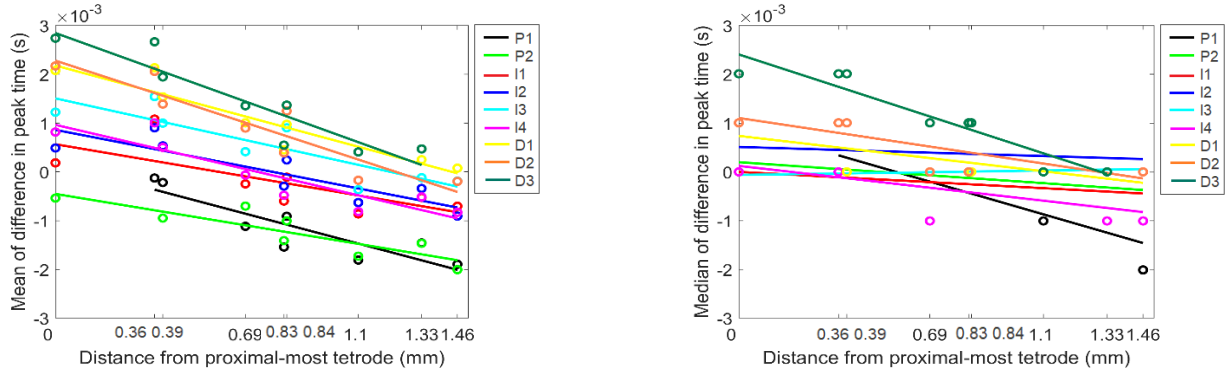

b) rat 432 : day 2 session 1

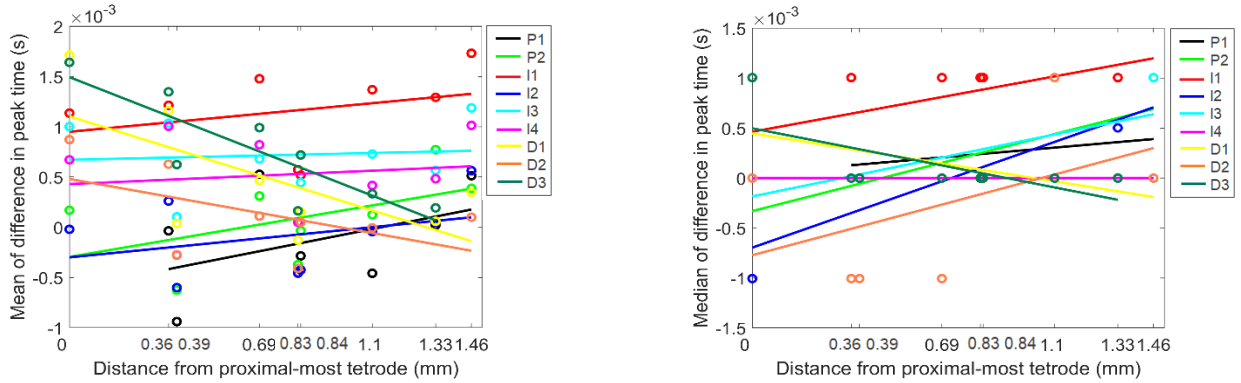

c) rat 432 : day 2 session 2

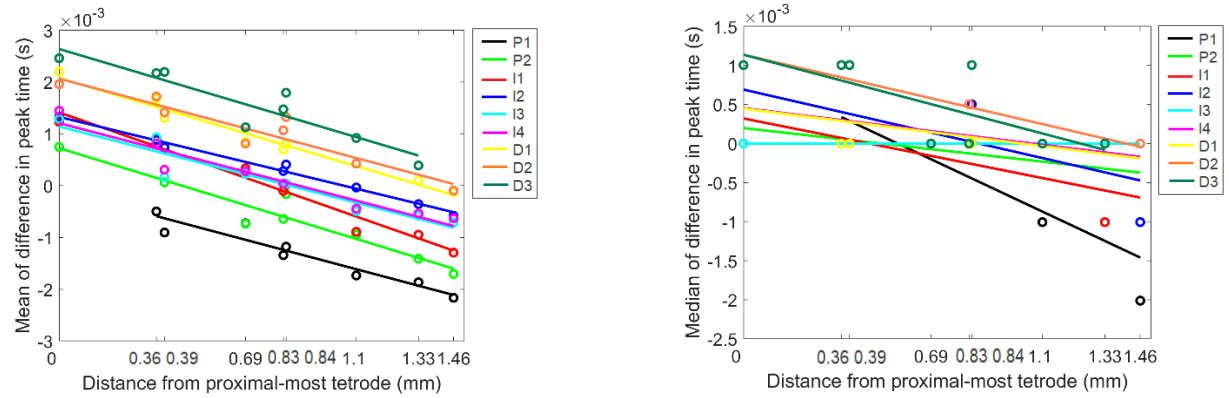

Fig. 19. Differences in peak time between referred tetrodes and reference tetrodes for rat 432 for the different sessions across days. Means (left) and medians (right) of the distributions with regression analysis for each reference tetrode plotted as a function of distance (each colour corresponds to a single reference tetrode).

rat 441 : day 1 session 1

a)

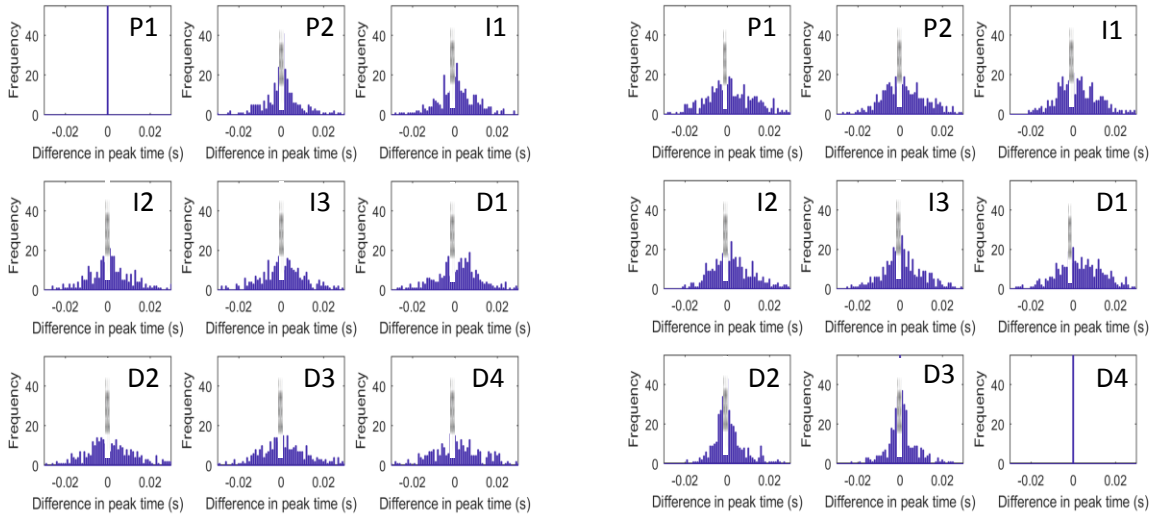

b)

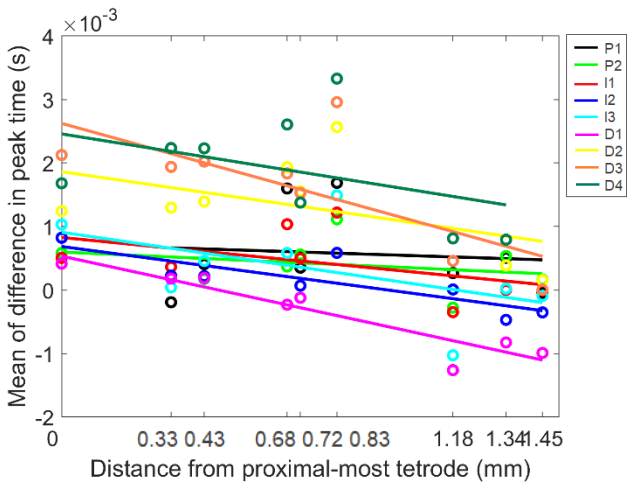

Fig. 20. Differences in peak time between referred tetrodes and reference tetrodes for rat 441.

a) Distributions of differences in peak time for each referred tetrode with respect to the proximal-most tetrode (left) and distal-most tetrode (right).

b) Means of the distributions with regression analysis for each reference tetrode plotted as a function of distance (each colour corresponds to a single reference tetrode).

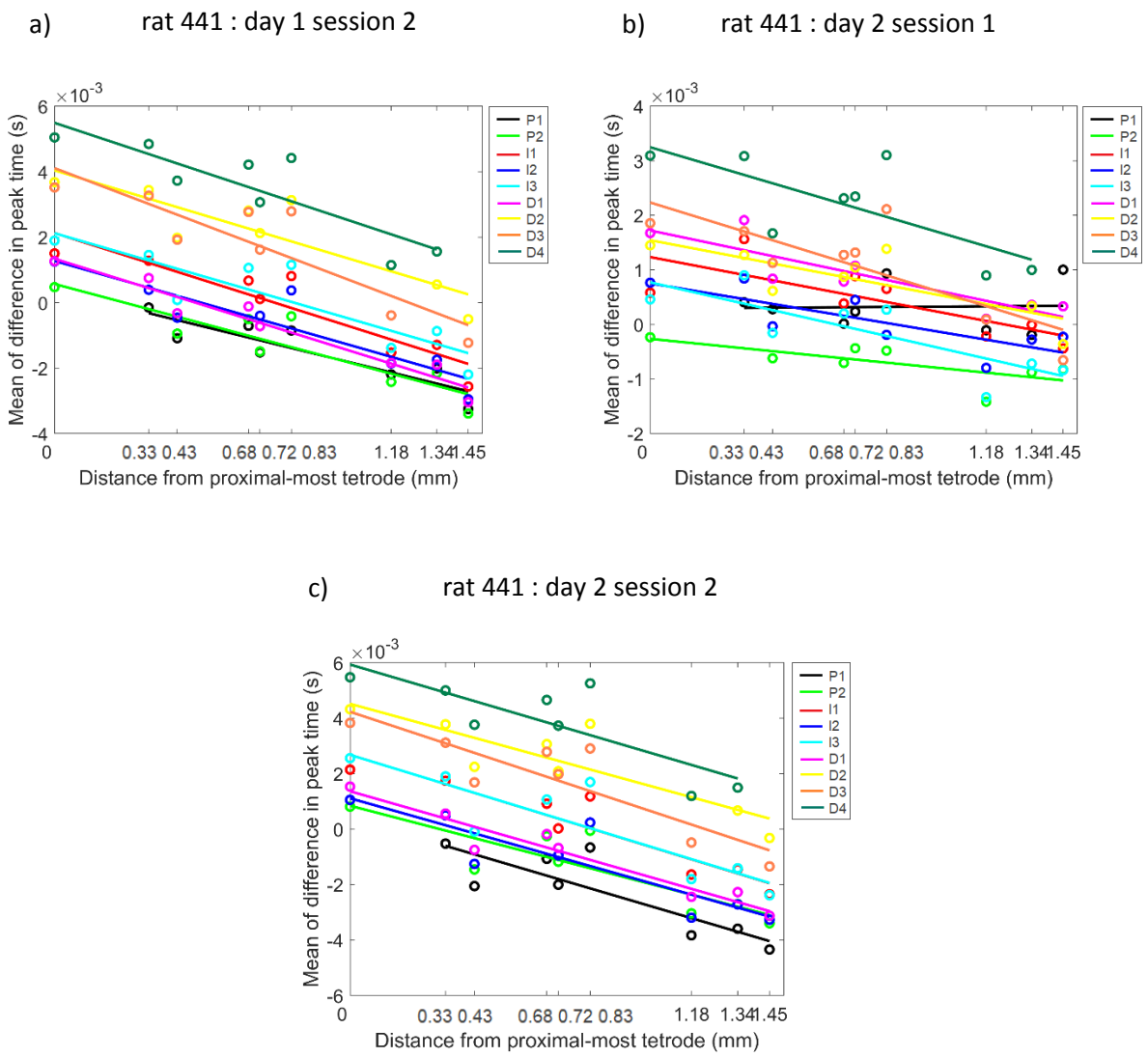

Fig. 21. Differences in peak time between referred tetrodes and reference tetrodes for rat 441 for the different sessions across days. Means of the distributions with regression analysis for each reference tetrode plotted as a function of distance (each colour corresponds to a single reference tetrode).

The result obtained was unlike what we expected – although ripples detected on any given reference tetrode were of relatively high amplitude (as seen in section 2 of Results), the relative time of occurrence of ripples in a given tetrode did not seem to depend on the relative amplitude. This was ascertained by looking at the peak time difference in occurrence of ripples that corresponded to the ripples that fell in the top 30 percentile of the range of relative amplitudes. As in section 2 of Results, the ripples that met this

criterion were pooled across sessions and days for each rat. The shift in the peaks of the distributions was more evident (Fig. 17(a), Fig. 18(a)), and trends in means of the distribution of time difference persisted and were significant (with correction for multiple comparisons) for rat 432 (proximal-most reference: $p = 0.00055$, $r^2 = 0.88$, distal-most reference: $p = 0.0011$, $r^2 = 0.85$) (Fig. 17(b)) and were significant (with correction for multiple comparisons) for the distal-most reference tetrode for rat 441 (proximal-most reference: $p = 0.206$, $r^2 = 0.25$, distal-most reference: $p = 0.0024$, $r^2 = 0.8$) (Fig. 18(b)).

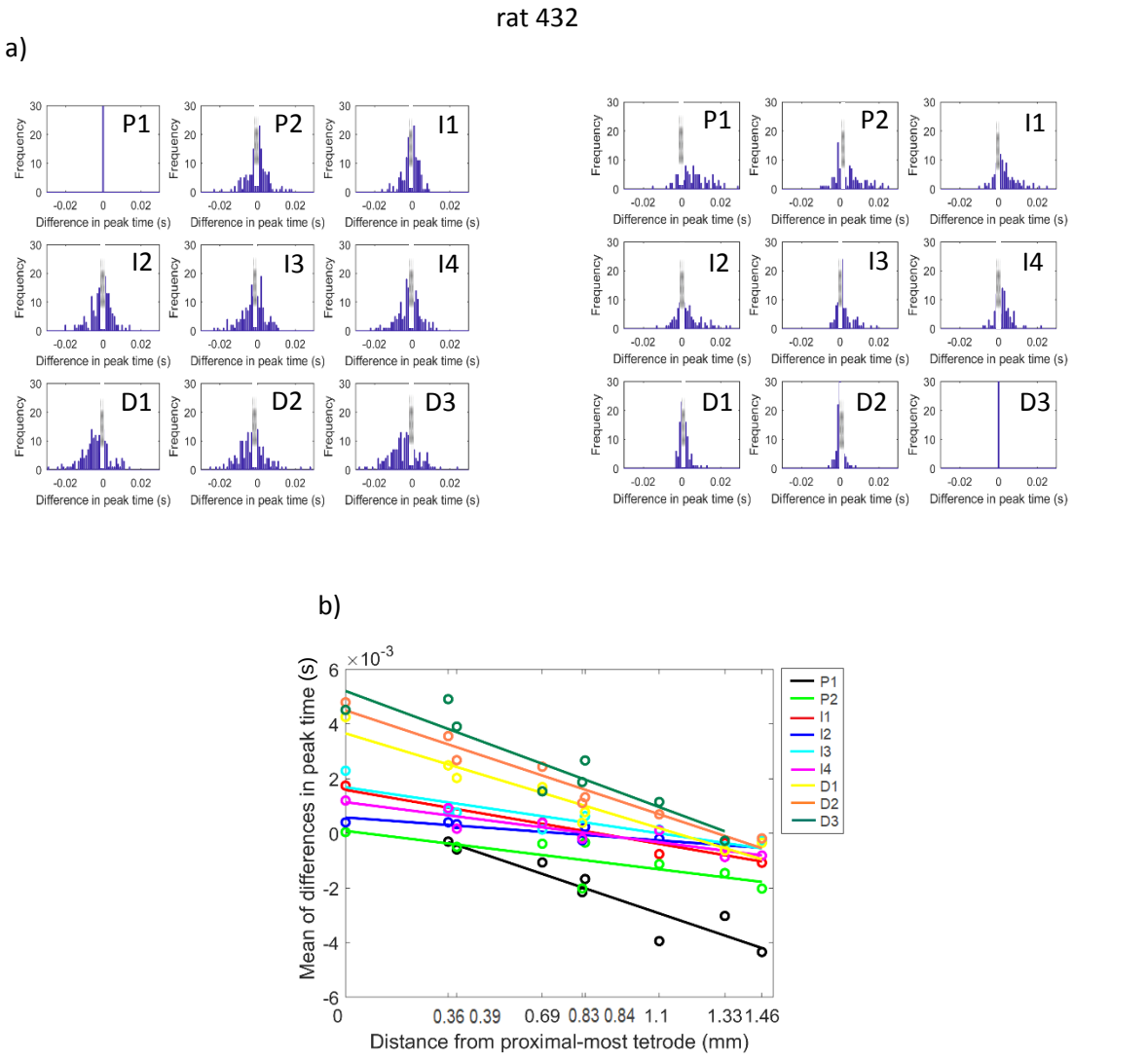

Fig. 22. Difference in peak time between referred tetrodes and reference tetrodes computed for ripples on reference tetrodes whose amplitude fell in the top 30 percentile, for rat 432. Means of the distributions with regression analysis for each reference tetrode are plotted as a function of distance.

rat 441

a)

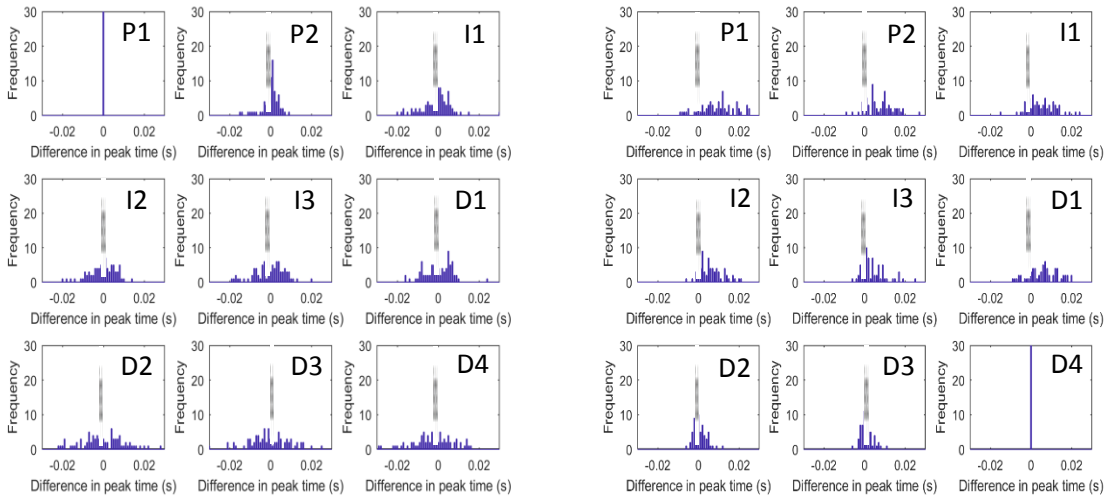

b)

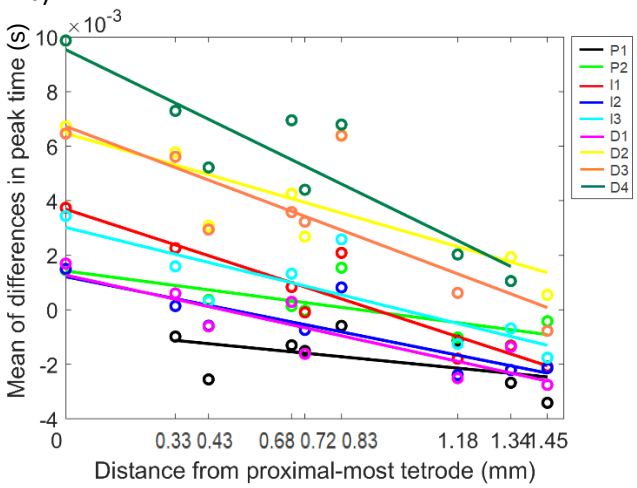

Fig. 23. Difference in peak time between referred tetrodes and reference tetrodes computed for ripples on reference tetrodes whose amplitude fell in the top 30 percentile, for rat 441. Means of the distributions with regression analysis for each reference tetrode are plotted as a function of distance.

Thus, it appears that ripples in distal CA1 may occur earlier than those in proximal CA1. This trend seems to become more prominent when relatively high amplitude ripples occur on reference tetrodes in both the proximal and distal regions. This differs from our expectation. Also, since the shift in the peaks of the distribution are not evident before

considering the ripples that fall in the top 30 percentile of relative amplitudes, it possible that ripples in other ranges of relative amplitudes have differing gradients in peak time difference. Hence, further analyses on this front are requisite to confirm these findings.

DISCUSSION

Analysis of SWR across the proximal-distal axis of area CA1 of the hippocampus shows that there are differences in their characteristics across the proximal and distal regions despite the rates of their occurrence being similar across the proximal-distal axis. We found clear trends in the co-occurrence of SWR across the proximal-distal axis. When SWR occurred on any tetrode of proximal CA1, SWR were more likely to co-occur on tetrodes that were closer to proximal CA1, and this likelihood reduced as we traversed to distal CA1. Likewise, when SWR occurred on any tetrode on intermediate or distal CA1, SWR were more likely to co-occur on other tetrodes closer to intermediate and distal CA1 respectively, as compared those on tetrodes that were further away. The likelihood of co-occurrence reduced along the proximal-distal axis from the point of reference, however, it did not fall to zero. This indicates that at any given time, SWR were not entirely localised to one region of area CA1.

We found that, more often than not, SWR did co-occur across the proximal-distal axis of area CA1. However, events that did co-occur in one region with those in another, could not always be detected using a single threshold (6 standard deviations); a lower threshold was required to detect these events (2 standard deviations). This could possibly imply that as we go from one region of area CA1 to the others, the amplitude of the ripple goes down. This possibility was confirmed when we investigated how the amplitude of ripples varies across the proximal-distal axis. Ripple amplitudes followed trends similar to that of co-occurrence, i.e. when ripples occurred on a tetrode in a given region of CA1, the relative amplitudes on other tetrodes corresponding to these ripples was higher for those that were closer to the given region than those that were further away. Thus, relatively high amplitude ripples occurred and were detected across the proximal-distal axis, however, the relatively high amplitude ripples in one region did not necessarily coincide with those in the other regions. This could indicate that SWR are initiated in any one

region and progressively travel to the other regions. The connectivity within area CA1 is known to be sparse (Christian and Dudek, 1988), thus, the possible travel of SWR is not likely due to a direct interaction between one region of area CA1 with another. It could be a reflection of the CA3 network activity, as CA3 is believed to drive SWR in area CA1. The recurrent connections in area CA3 are believed to give rise to a large number of synchronously firing neurons in distal CA3 (reviewed in Buzsáki, 2015). This increased neuronal activity has been shown to propagate to proximal CA3, and subsequently to area CA1 (Csicsvari et al., 2000). Since proximal CA3 projects to distal CA1 and distal CA3 projects to proximal CA1, we can expect the neuronal activity (and consequently, the amplitude of ripples) in the proximal and distal CA1 to parallel the input received from distal and proximal CA3 respectively. The higher density of recurrent connections in distal CA3 would be expected to give rise to a greater number of synchronously firing neurons in distal CA3 as compared to proximal CA3, whose recurrent connectivity is sparse. Also, considering the fact that the projections from distal CA3 to CA3 become sparser towards proximal CA3, one would expect an attenuation in the propagation of synchronous firing of neurons towards proximal CA3. Greater synchrony in distal CA3 could give rise to greater synchrony of neuronal firing in proximal CA1, and lesser synchrony in proximal CA3 could give rise to lesser synchrony of neuronal firing in distal CA1. This would possibly give rise to larger amplitude ripples in proximal CA1 as compared to distal CA1, which could provide a possible explanation for one of the gradients in amplitude viz. the decreasing gradient in relative amplitude of ripples from proximal CA1 to distal CA1. The recurrent network in distal CA3, however, does not seem sufficient to explain the other gradient in amplitude viz. the decreasing gradient in relative amplitudes that we see from distal CA1 to proximal CA1.

The recurrent connectivity in proximal CA3 could initiate synchronous firing of neurons in proximal CA3, and give rise to ripples in distal CA1, albeit of relatively low amplitude due to its sparse recurrent connectivity. Since projections from proximal CA3 to CA3 are more restricted to proximal CA3, we can expect that the synchronous firing initiated in proximal CA3 would get attenuated towards distal CA3, as in the above case. Ripples in proximal CA1 would then be of lower amplitude than those in distal CA1, even though the activity

initiated by proximal CA3 is generally expected to be of low amplitude. In this manner, the network activity in area CA3 could explain the decreasing gradient in relative amplitude that we see from distal CA1 to proximal CA1 too.

A progression of synchronous neuronal activity from one region of area CA3 to another across its proximal-distal axis implies that there would be a time-lag between the neuronal activity between the region of initiation and the regions further away from this region in area CA3. A corresponding time-lag would be expected across the proximal-distal axis of area CA1 – if synchronous firing of neurons is initiated in distal CA3, SWR in proximal CA1 would be expected to occur earlier than the corresponding ones in distal CA1, and vice versa. Surprisingly, we found that the peak time differences in SWR showed that SWR tend to occur earlier in distal CA1, irrespective of which region had relatively high amplitude ripples. Our observations of the distributions of differences in peak time did not always corroborate this result. However, considering the possibility that our result is genuine, we could provide possible explanations for the same. The phenomenon of synchronous firing being initiated by proximal CA3 would be expected to be relatively infrequent as compared to distal CA3 initiating the same due to the sparse recurrent connectivity in proximal CA3 (and also reported by Csicsvari et al. 2000). Therefore, it is unlikely that the time gradient that we see from distal CA1 to proximal CA1 is the outcome of a majority of the SWR being initiated by proximal CA3. Considering the large amount of recurrent connectivity in distal CA3, it is likely that the synchronous firing increases to a greater extent in distal CA3 than proximal CA3 over a relatively longer duration of time during a ripple event, before it reduces. This could be reflected in the ripples in area CA1, resulting in the peak of the ripples in proximal CA1 to occur later than those in distal CA1, even if distal CA3 gives rise to ripples earlier in proximal CA1.

In addition to area CA3, the entorhinal cortex also projects to area CA1. Sharp-waves and ripples in the entorhinal cortex, however, have been shown to occur either simultaneously or 5 – 30 ms after those that occur in area CA1 (Chrobak and Buzsáki, 1996). Also, Chrobak and Buzsáki (1994) have shown that neurons in the layers of MEC that project to area CA1 (layers II and III) do not increase their firing during SWR in area CA1. This suggests that the contribution of the MEC may not be much to the initiation of

SWR. In contrast to this finding, Sullivan et al. (2011) have shown a relative increase in the firing of neurons in layers II and III of the MEC during SWR. Thus, the MEC may play some role in SWR. The influence of the lateral entorhinal cortex (LEC) on SWR has not been much studied. We can, however, speculate the possible role of the LEC in SWR.

Considering the possibility that the MEC and LEC play a role in SWR in area CA1, they might contribute in the following ways. The MEC projects to proximal CA1, and to a greater extent to distal CA3 than proximal CA3. In conjunction with the recurrent connections in area CA3, the increased neuronal firing in MEC could give rise to synchronous firing in distal CA3. The increased firing in the MEC could also drive SWR in proximal CA1. This could give rise to two possibilities. If the MEC and distal CA3 activate neurons in a co-ordinated manner so as to give rise to synchronous firing of neurons in proximal CA1, one would expect relatively larger amplitude ripples in proximal CA1 as compared to distal CA1 (which is driven by proximal CA3). On the other hand, there is also the possibility that the drive to proximal CA1 from distal CA3 and the MEC may not be concerted, which could disrupt synchrony in proximal CA1. This could give rise to relatively low amplitude ripples in proximal CA1, while distal CA1 has relatively higher amplitude ripples due to the synchronous firing driven by proximal CA3. Similarly, the LEC, which projects to distal CA1, and to a greater extent to distal CA3 than proximal CA3, could either give rise to relatively high amplitude ripples in distal CA1 if it activates neurons in co-ordination with proximal CA3, or give rise to relatively low amplitude ripples if it does not activate neurons in distal CA1 in concert with proximal CA3.

The possible contribution by the LEC could explain the occurrence of a portion of the ripple peaks being earlier in distal CA1. The LEC could directly activate neurons in distal CA1, initiating ripples in distal CA1 relatively earlier. On the other hand, we would expect the MEC to initiate ripples earlier in proximal CA1. However, since entorhinal cortical activity is expected to activate area CA3 as well, the entorhinal cortex, along with area CA3 may give rise to entirely different peak time differences. To confirm whether our result and speculations are commensurate with the actual phenomenon, we could look at whether the trends in the difference in time at which the ripple events start are different from those of the difference in peak time over the proximal-distal axis of area CA1. We

could also look at the entire duration of ripples and also the duration from the start time to the peak time across the proximal-distal axis of area CA1; this could inform us whether the recurrent connectivity in distal CA3 does indeed build up the synchronous firing of neurons over a longer duration of time than that of proximal CA3.

The differences in SWR across the proximal-distal axis of area CA1 provide some insight into the possible dynamics of the networks involving area CA3 and the entorhinal cortex that connect to area CA1. Our attempt at inferring the network dynamics, however, has been restricted to what the relative amplitudes tell us. Since we do not have any information regarding the absolute amplitudes of ripples across the proximal-distal axis of area CA1, we cannot rule out the possibility that the amplitude of ripples may always be higher in one region than the other. This could change our inferences and understanding of the network dynamics. Another thing that could alter our understanding of the network dynamics is changing our approach towards looking at differences in time of ripples across the proximal-distal axis of area CA1. Instead of averaging the time difference over all events, we could separately look at SWR that occur earlier and later with respect to the SWR on the reference tetrode. Patel et al. (2013) have employed a method along these lines to look at the progression of SWR across the septo-temporal axis effectively. Additionally, they have looked at the probability of co-occurrence and amplitudes of ripples across the septo-temporal axis. Their approach to carrying out these analyses are different from ours, therefore, it may be useful to adopt their methods of analyses in order to refine ours.

Apart from this, the study by Patel et al. (2013) on SWR across the septo-temporal axis is of importance to us as our hyperdrive did spanned the septo-temporal axis to some extent (0.8 – 1 mm). They have shown that the probability of co-occurrence decreased with increasing distance across the septo-temporal axis as we saw across the proximal-distal axis. The probability of co-occurrence across the septo-temporal axis seemed to decrease by about 40% with increasing distance, in the range of 0 – 2 mm. Hence, SWR dynamics exist along the septo-temporal axis as well, and it would be of interest to us to look at differences in SWR in two dimensions rather than one dimension to interpret our

results better and gain a more nuanced understanding of the possible dynamics of the network that connects to area CA1.

To gain a more extensive understanding of the network dynamics, it would also be essential to study the dynamics of SWR in conjunction with neuronal activity during the experimental sessions. Since neurons that fire during behaviour are known to fire during SWR too (reviewed in Buzsáki 2015), SWR dynamics during immobility and sleep may be dependent on the neuronal activity during behaviour. The results we have obtained are exclusive to one experimental paradigm. Paradigms such as those used by Henriksen at al. (2010), Igarashi et al. (2014), and Nakazawa et al. (2016) have each shown differential neuronal activity across the proximal-distal axis of area CA1 during behaviour, from one another. Therefore, SWR dynamics during immobility and sleep may be different for each of these paradigms. It would be useful to us to study SWR dynamics with respect to a multitude of such paradigms and link it to the neuronal activity during behaviour. Another factor to consider is that our rats were exposed to the experimental setup prior to the experiment. The rate of occurrence of SWR and the neuronal activity associated with SWR have been shown to differ depending on experience (reviewed in Buzsáki, 2015). Hence, it would also be useful to compare SWR dynamics prior to the exposure to a novel environment, after the exposure to the novel environment, and once familiarisation has taken place. While carrying out these recordings, it would be beneficial to simultaneously record and look at neuronal activity from the entorhinal cortex and area CA3 along with area CA1. In addition to this, it would be insightful to study how the gradients in ripple amplitude and differences in time vary in time i.e. we can look at the spatio-temporal dynamics of SWR. This could inform us about whether there are switches in the activity of the network in different regions of area CA3 and possibly, the entorhinal cortex.

Thus, there are a number of aspects of the dynamics of SWR in area CA1 that are yet to be understood in order comprehend the dynamics of the network that connects to area CA1. Nonetheless, our results have established that there are differences in the activity of the network which can be used as a basis for carrying out further studies.

REFERENCES

Buzsáki, G., Leung, L.S., and Vanderwolf, C.H. (1983). Cellular basis of hippocampal EEG in the behaving rat. Brain Res. Rev. *6*, 139–171.

Buzsáki, G. (1986). Hippocampal sharp waves: their origin and significance. Brain Res. *398*, 242–252.

Buzsáki, G., Horváth, Z., Urioste, R., Hetke J., and Wise K. (1992). High-frequency network oscillation in the hippocampus. Science *256*, 1025–1027.

Buzsáki G. (2015). Hippocampal sharp wave-ripple: a cognitive biomarker for episodic memory and planning. Hippocampus *25*, 1073–1188.

Christian, E.P., and Dudek, F.E. (1988). Electrophysiological evidence from glutamate microapplications for local excitatory circuits in the CA1 area of rat hippocampal slices. J. Neurophys. *59*, 110–123.

Chrobak, J.J., and Buzáski, G. (1994). Selective activation of deep layer (V-VI) retrohippocampal cortical neurons during hippocampal sharp-waves in the behaving rat. J. Neurosci. *14,* 6160–6170.

Chrobak, J.J., and Buzsáki, G. (1996). High-frequency oscillations in the output networks of the hippocampal-entorhinal axis of the freely behaving of the rat. J. Neurosci. *16*, 3056–3066.

Csicsvari, J., Hirase, H., Czurko, A., Mamiya, A., and Buzsáki, G. (1999). Oscillatory coupling of hippocampal pyramidal cells and interneurons in the behaving rat. J. Neurosci. *19*, 274–287.

Csicsvari, J., Hirase, H., Mamiya, A. and Buzsáki, G. (2000). Ensemble patterns of hippocampal CA3-CA1 neurons during sharp wave - associated population events. Neuron *28*, 585–594.

Deshmukh, S.S., and Knierim, J.J. (2012). Hippocampus. WIREs Cogn. Sci. *3*, 231–251.

Eschenko, O., Ramadan, W., Mölle, M., Born, J., and Sara, S.J. (2008) Sustained increase in hippocampal sharp-wave ripple activity during slow-wave sleep after learning. Learn. Mem. *15*, 222–228.

Girardeau, G., Benchenane, K., Wiener, S.I., Buzsáki, G., and Zugaro, M.B. (2009). Selective suppression of hippocampal ripples impairs spatial memory. Nat. Neurosci. *12*, 1222–1223.

Henriksen, E.J., Colgin, L.L., Barnes, C.A., Witter, M.P., Moser, M., and Moser, E.I. (2010). Spatial representation along the proximodistal axis of CA1. Neuron *68*, 127–137.

Igarashi, K.M., Lu, L., Colgin, L.L., Moser, M., and Moser, E.I. (2014). Coordination of entorhinal–hippocampal ensemble activity during associative learning. Nature *510,* 143–147.

Ishizuka, N., Weber, J., and Amaral, D.G. (1990). Organization of intrahippocampal projections originating from CA3 pyramidal cells in the rat. J. Comp. Neurol. *295*, 580–623.

Karlsson, M.P., and Frank, L.M. (2009). Awake replay of remote experiences in the hippocampus. Nat. Neurosci. *12*, 913–918.

Komorowski, R.W., Manns, J.R., and Eichenbaum H. (2009). Robust conjunctive item-place coding by hippocampal neurons parallels learning what happens where. J. Neurosci. *29*, 9918 –9929.

Li, X.G., Somogyi, P., Ylinen, A., and Buzsaki, G. (1994). The hippocampal CA3 network: an *in vivo* intracelluar labelling study. J. Comp. Neurol. 339, 181–208.

Mitra, P.P., and Pesaran, B. (1999). Analysis of dynamic brain imaging data. Biophys. J. *76*, 691–708.

Moita, M.A.P., Rosis, S., Zhou, Y., LeDoux, J.E., and Blair, H.T. (2003). Hippocampal place cells acquire location-specific responses to the conditioned stimulus during auditory fear conditioning. Neuron *37*, 485–497.

Naber, P.A., Lopes Da Silva, F.H., and Witter, M.P. (2001). Reciprocal connections between the entorhinal cortex and hippocampal fields CA1 and the subiculum are in register with the projections from CA1 to the subiculum. Hippocampus *11*, 99–104.

Nakazawa, Y., Pevzner, A., Tanaka, K.Z., and Wiltgen, B.J. (2016). Memory retrieval along the proximodistal axis of CA1. Hippocampus *26*, 1140–1148.

O'Keefe, J. (1976). Place units in the hippocampus of the freely moving rat. Exp. Neurol. *51*, 78–109.

Patel, J., Schomburg, E.W., Berenyi, A., Fujisawa, S., and Buzsáki, G. (2013). Local generation and propagation of ripples along the septotemporal axis of the hippocampus. J. Neurosci. *33*, 17029–17041.

Scoville, W.B., and Milner, B. (1957). Loss of recent memory after bilateral hippocampal lesions. J. Neurol. Neurosurg. Psychiatry *20,* 11–21.

Skaggs, W.E., McNaughton, B.L., Wilson, M.A., and Barnes, C.A. (1996). Theta phase precession in hippocampal neuronal populations and the compression of temporal sequences. Hippocampus *6*, 149–172.

Sullivan, D., Csicsvari, J., Mizuseki, K., Montgomery, S., Diba, K., and Buzsáki, G. (2011). Relationships between hippocampal sharp waves, ripples, and fast gamma oscillation: influence of dentate and entorhinal cortical activity. J. Neurosci. *31*, 8605–8616.

Suzuki, S.S., and Smith, G.K. (1988). Spontaneous EEG spikes in the normal hippocampus. IV. Effects of medial septum and entorhinal cortex lesions. Electroencephalogr. Clin. Neurophysiol. *70*, 73–83.

Tamamaki, N., and Nojyo, Y. (1995). Preservation of topography in the connections between the subiculum, field CA1, and the entorhinal cortex in rats. J. Comp. Neurol. *353*, 379–390.

van Strien, N.M., Cappaert, N.L.M., and Witter, M.P. (2009). The anatomy of memory: an interactive overview of the parahippocampal-hippocampal network. Nat. Rev. Neurosci. *10*, 272–282.

Witter, M.P. (2007). Intrinsic and extrinsic wiring of CA3: Indications for connectional heterogeneity. Learn. Mem. *3*, 705–713.

Ylinen, A., Bragin, A., Nadasdy, Z., Jando, G., Szabo, I., Sik, A., and Buzsáki, G. (1995). Sharp wave-associated high-frequency oscillation (200 Hz) in the intact hippocampus: network and intracellular mechanisms. J. Neurosci. *15*, 30-46 .